nature portfolio

Peer Review File

Probing Far-From-Equilibrium Dynamics of Electrical Double Layers

Corresponding Author: Professor Tao Wang

Any redactions in this file are there to maintain patient confidentiality, the confidentiality of unpublished data, or to remove third-party material.

This file contains all reviewer reports in order by version, followed by all author rebuttals in order by version.

Version 0:

Reviewer comments:

Referee #1

(Remarks to the Author)
The paper presents the concept of EDL breathing, a dynamic process in which the electrical double layer at the solid-liquid interface undergoes cyclic contraction and expansion under potential step experiments. Using SEIRAS, the authors observe changes in water structure and ion distributions, linking these phenomena to dehydration and rehydration during contraction and expansion phases.

Specific comments:

1)Electrostriction is a well-known phenomenon in which the electrical double layer contracts under applied bias, but this is not mentioned in the paper. This effect is well documented in older works by Conway, Bockris, and others and should be acknowledged and discussed. Relevant references include 10.1039/CS9922100253 and 10.1021/cr100130d.How is what is observed in this paper different than electrostriction?

2) During the SEIRAS measurements, the authors presumably collected steady-state current versus time traces (at constant voltage) as well as voltammograms. This data should be included in the paper and discussed alongside the SEIRAS data to provide a more complete picture of the system's behavior.

3) The authors state, "Interestingly, the intensity of this band at 750 ms is approximately 1.5 times higher than in the steady state (>3000 ms), indicating a disordered water network in the transition state." Why is this true? More details on how this conclusion is justified would be helpful. Currently, it is stated without a detailed explanation. It is well documented that water solvated to alkali metal cations (such as sodium) exhibits an O-H vibrational frequency around 3600 cm^{-1}. Is ion-solvated water truly disordered? Furthermore, the free water mode still involves on hydrogen bonded OH molecule. The O-H vibration in "free water" is energetically uncoupled from the H-bonded O-H groupReferences such as Wang et al. (Nature, 2021, 600, 81-85) and Scatena et al. (Science, 2001, 292, 908-912)

4)SEIRAS data collected in alkali-metal-free electrolytes down to -1.1 V, along with time-resolved measurements similar to those in Figure 2, is missing. This data is necessary to determine whether the "breathing behavior" is specific to alkali-metal-containing systems or is a general phenomenon. Additionally, it would help clarify how alkali metals influence the behavior of the interface.

5) The authors show simulated concentrations of K^+ at the outer layer and the surface in Figure 4f. What is the maximum surface coverage of cations that can be adsorbed on the electrode under large negative bias? Does the model, which includes inner layer contraction, accurately predict these maximum coverages?

6) The authors observe irreversible behavior, as the water does not completely return to its original state upon reversal of the potential. Why does this irreversibility occur? Can the authors propose a hypothesis to explain this observation?

7) The authors discuss differences in the electric fields experienced by CO and Pt-H species on the electrode surface, yet

the distance between these two molecules is not explicitly provided. Is this distance truly significant enough to account for the difference in electric field intensity? Alternatively, could the observed behavior arise from CO and Pt-H occupying distinct adsorption sites on the electrode? Furthermore, the assertion that CO coverage is only at 1% warrants clarification.

Referee #2

(Remarks to the Author)
The manuscript discusses the preparation and characterisation of platinum nanofilm electrodes for use in electrochemical measurements and surface-enhanced infrared absorption spectroscopy (SEIRAS). Using this methodology, the impact of ion interactions on the dynamics of the electric double layer during hydrogen evolution at negative potentials was studied. It particularly highlights how the presence of cations in the electrolyte influences the structure of interfacial water and the dynamics of such a structure during potential variation. The study is complemented with DFT calculations of both the double-layer structure and vibrational contributions of interfacial water and with a mean field model based on the Poisson-Boltzmann equation to explain the changes in the electric field inferred from the Stark effect on the vibrations of adsorbed hydrogens. The manuscript is well written, and the hypothesis proposed to explain the spectroscopic observations is reasonable. I have one major concern: How can the authors rule out local changes at the interphase induced by hydrogen evolution as the cause of some spectroscopic observations? I refer to bubble formation and local pH changes. Such effects should be considered with caution. Other minor point are: -While all potentials in the text are given with reference to the standard hydrogen electrode, the only voltammogram shown in the Supporting Information is plotted versus the calomel reference electrode. This makes it difficult to correlate the spectroscopic results with the electrochemical response of the electrode. -While the voltammogram looks clean and compatible with a clean interphase, I am worried that some lead used in the electroplating solution might be alloyed with platinum and might affect the rate of hydrogen evolution. Have the authors checked the films for the presence of lead by XPS or related techniques? -Finally, in Supplementary Note 7, the authors claim that both underpotential and overpotential hydrogen are visible in the spectra, while I can only see one band in the spectra. This requires clarification. Besides, the coverage of 66% that the authors mention is only valid for Pt(111), while the voltammogram shows a response corresponding to polycrystalline platinum, where coverage is close to 100%. Therefore, the reference to the value of 66% might be irrelevant in this case.

Version 1:

Reviewer comments:

Referee #1

(Remarks to the Author)
This revision of the manuscript mostly addresses the comments and the authors give many experimental/computational data to again support their observation. There are some minor points that I would still like to point out for the authors' attention.

1) In Figure 3, a ~800 ms temporal range is observed for Phase I-to-II transition. The authors state that this transition and related spectral data are due to inner Helmholtz plane contraction, or "breathing". With MLMD-simulated spectra, this conclusion is indeed reasonable, but in a more general physical picture, HER on Pt catalyst should mainly be a diffusion-controlled process. Thus, diffusion length can be derived from random walk process in the form of l^2~D·τ. So we can actually qualitatively evaluate the diffusion length within ~800 ms with a common D of 10-5 cm2/s, where l~28 um. This is somehow much larger than how the spatial scale of inner Helmholtz layer should be, often in Å scale. The rough estimation should remind us of considering whether EDL is actually being compressed in the inner layer or it is just reconstructuring its network. Also the contraction length is just about 2 Å from SI Fig. S 27. Though my consideration doesn't has to be completely correct, so a clarification from the authors is necessary to convince readers.

2) Other minor points are just some typos or unclear sentences in the manuscript. Line 66—an additionaly underline during sentences. "reaction conditions._Consequently, " Extended Fig 2—adding electrolyt information could be clearer for readers. SI Fig. S 4—caption and figure don't match with each other.

(Remarks on code availability)

Referee #2

(Remarks to the Author)
The authors have convincingly addressed all of my comments. I find the paper to be robust, presenting very interesting results, and it can be published mainly in its current form. However, there is one aspect that I believe still requires clarification to enhance the manuscript's readability. This is related to the direction (positive or negative) of the vibrational bands. While the manuscript clearly states that positive bands indicate a decrease in the population of species from reference to sample potential, I feel the discussion becomes somewhat unclear at some points. For instance, the positive band at 3600 cm-1 observed during the desolvation of cations at very negative potentials should be interpreted as a signal of non-hydrogen bonded water molecules present at the reference potential, which is 0.37 V. Typically, an ice-like water structure has been reported in this potential range, and I am not aware of any previous detection of such non-bonded water around this potential. If this water signal pertain to water in the first or second solvation layer of the cation, it should be present at the reference potencial, which is slightly positive to the potential of zero charge

For instance, in page 8 we read the following paragraph: " In the second phase, the interfacial structure deviates significantly from equilibrium. A distinct shift of the upward peak from 3568 cm-1 to 3492 cm-1 is observed, with intensity increasing as potential becomes more negative. This spectral evolution is attributed to the contraction of the inner layer, as captured by simulations, indicating a reduced interfacial water content (Fig 2g-j). As shown in Fig 2m, the hydration shell of K^+ remains largely unchanged during phase I but undergoes notable changes in phase II. As potential decreases, the surface coverage of K^+ increases, and its second hydration shell (~5 Å) is significantly disrupted. Simultaneously, a decrease in the first hydration shell peak suggests partial dehydration of K^+. " As I mentioned earlier, the upward peak originates from a signal present at the reference potential. It remains unclear how the dehydration of potassium alone can account for this, given that potassium cations must be absent at the reference potential because it is above the pzc.

Appart from this clarification, the paper can be published in its present form.

(Remarks on code availability)
The computational calculations described in this associated material are outside my area of expertise. I feel unable to make comments on this.

Version 2:

Reviewer comments:

Referee #1

(Remarks to the Author)
The authors have adequately addressed the comments. I have no further comments

(Remarks on code availability)

Referee #2

(Remarks to the Author)
The authors have answered my previous concern, so I think the ms. can now be published in the present form.

(Remarks on code availability)

Open Access This Peer Review File is licensed under a Creative Commons Attribution 4.0 International License, which permits use, sharing, adaptation, distribution and reproduction in any medium or format, as long as you give appropriate credit to the original author(s) and the source, provide a link to the Creative Commons license, and indicate if changes were made.
In cases where reviewers are anonymous, credit should be given to 'Anonymous Referee' and the source.

The images or other third party material in this Peer Review File are included in the article's Creative Commons license, unless indicated otherwise in a credit line to the material. If material is not included in the article's Creative Commons license and your intended use is not permitted by statutory regulation or exceeds the permitted use, you will need to obtain permission directly from the copyright holder.
To view a copy of this license, visit https://creativecommons.org/licenses/by/4.0/

Reviewers' comments:

Reviewer #1:

The paper presents the concept of EDL breathing, a dynamic process in which the electrical double layer at the solid-liquid interface undergoes cyclic contraction and expansion under potential step experiments. Using SEIRAS, the authors observe changes in water structure and ion distributions, linking these phenomena to dehydration and rehydration during contraction and expansion phases.

Response:

We would like to thank this reviewer for the careful evaluation and valuable comments of this study.

Specific comments:

Comment 1: Electrostriction is a well-known phenomenon in which the electrical double layer contracts under applied bias, but this is not mentioned in the paper. This effect is well documented in older works by Conway, Bockris, and others and should be acknowledged and discussed. Relevant references include 10.1039/CS9922100253 and 10.1021/cr100130d.How is what is observed in this paper different than electrostriction?

Response:

We thank the reviewer for this constructive comment. and bringing our notice to earlier works on electrostriction which were unintentionally missed in our previous manuscript but are cited and commented in the revised manuscript. We argue below that the EDL breathing in this study goes substantially beyond the electrostriction in the literature.

Electrostriction, first introduced by Drude and Nernst in the 19th century, describes the volume contraction of materials under an electric field[1]. In electrochemistry, it refers to the electrostatic compression of solvents by electrolyte ions, such as the disruption of aqueous hydrogen-bond networks[1]. Ions can generate electric fields up to 10^7 V cm^{-1}, producing electrostrictive pressure detectable through precise solution property measurements[2]. While bulk electrostriction is well understood, its behavior at the electrical double layer (EDL), where electrocatalysis occurs, remains poorly explored. At the EDL, electrostriction arises from the interplay between short-range ion-solvent interactions and long-range electrode fields, jointly determining ion configurations and field distributions. As Conway noted, comparing electrostriction of ions with that of solvents in the EDL is of great interest, yet direct volumetric measurement on the key quantity, ΔV_e^o, values (per cm^2), at electrode/solution interfaces, especially for

electrocatalytic condition, is experimentally very challenging[2].

More importantly, conventional electrostriction assumes a static, reversible response and overlooks far-from-equilibrium interfacial dynamics. In contrast, we probed the EDL's dynamic structure under reactive conditions using time-resolved SEIRAS, revealing a potential-driven "EDL breathing" process involving structural/spatial rearrangements of hydrated cations and evolving electric field intensities. Compared with the classical picture of electrostriction, our work substantially advances the concept in three key aspects:

(1) Time-resolved measurement under reactive conditions. Electrostriction doesn't consider the time-dependent variation of EDL. By using Pt nanofilm electrodes for transient SEIRAS, which enhance interfacial signals and withstand HER conditions, we directly observed potential-driven EDL contraction and expansion dynamics, marking the first atomic-level evidence of "EDL breathing." Coupled with a compressible EDL model, we quantified the electric field evolution under non-equilibrium conditions, establishing a framework for electrolyte-engineered reactivity control.

(2) Resolving interfacial water dynamics. Electrostriction doesn't consider the detailed molecular picture, while a two-phase evolution of water structure during EDL contraction is captured in our work. Traditional IR peak deconvolution and AIMD simulations, often based on hydrophobic interfaces[3,4] and SEIRAS studies[5,6], capture hydrogen-bond structure under static state but fail to represent dynamic reactive interfaces where ion migration, solvent reorganization, dehydration, and complex field distributions coexist. We address this, newly added in the revision stage, by applying machine learning molecular dynamics (MLMD) to simulate charge fluctuations and solvent dynamics over nanoseconds with larger cells, yielding spectra that match SEIRAS data and accurately describe hydrogen-bond network evolution.

(3) Mapping spatially distributed electric fields. Electrostriction is still not incorporated into GCSC models, therefore the quantitative picture about how dehydrated cation influence the local electric field is still missing. We introduced four different interfacial probes to measure electric field intensities at multiple EDL positions during contraction. The compressible model reproduces these spatial variations, offering a full description of interfacial field evolution under reactive conditions.

In summary, while we fully acknowledge the importance of the early insights of electrostriction, our study experimentally captures the dynamic "EDL breathing" behavior, integrates MLMD for resolving interfacial water networks, and quantitatively maps spatial electric field distributions. These findings enrich the understanding of electrolyte effects, with implications for non-equilibrium electrocatalysis and emerging pulsed electrocatalysis strategies.

To enhance the discussion on electrostriction, we have added following discussion

in the revised manuscript (Page 3, Line 52-69):

"Despite significant progress, the underlying mechanism of the cation effect remains a topic of ongoing debate. Various theoretical frameworks have been proposed to explain this effect, focusing on factors such as the influence of local electric field distribution[6,7], non-covalent interactions between cations and reaction intermediates[10], and the role of interfacial water structures[17,21]. However, these effects are inherently coupled within EDLs, where changes in the local electric field, ion movement, and water molecule arrangement are interdependent. Therefore, a unified physical model of the dynamic EDL under reaction conditions is essential for quantitatively assessing these different contributions. Conway et al. previously emphasized the importance of electrostriction in interpreting ion size variations at electrochemical interfaces, highlighting its potential to capture field-induced compression effects[22-24]. However, the dynamic aspects of electrostriction at the molecular level remains largely unexplored under reactive conditions. In addition, an EDL model incorporating electrostriction effects is missing while invaluable for quantitative predictions of local reaction conditions. Consequently, the development of a time-dependent and reactive EDL framework is critical for reconciling the complex kinetic behaviors observed across different potential windows, and for establishing a comprehensive, molecular-level understanding of electrocatalytic processes."

Comment 2: During the SEIRAS measurements, the authors presumably collected steady-state current versus time traces (at constant voltage) as well as voltammograms. This data should be included in the paper and discussed alongside the SEIRAS data to provide a more complete picture of the system's behavior.

Response:

We thank the reviewer for this thoughtful comment. In the original submission, we presented potential-dependent SEIRAS spectra but did not include steady-state current and corresponding voltammograms. To provide a more comprehensive view of the EDL structure under reactive condition, we have now included these electrochemical data in the revised manuscript. Our steady-state SEIRAS experiments were conducted with a potential modulation program. In detail, SEIRAS spectra were continuously collected as the electrode potential was cycled between the reference potential and the working potentials. During this process, steady-state current versus time traces were automatically generated alongside the SEIRAS spectrum collection. The steady-state currents versus time traces, recorded between 0.37 V vs. SHE (reference potential) and different working potentials in a mixed solution of 0.1 M H_2SO_4 and 0.2 M K_2SO_4 have been shown in **Fig. R 1 a-k**. As the working potential decreased, both the HER current and the charging electric quantities of the EDL increased, indicating the accumulation of positive charges under HER conditions at the Pt electrodes. This trend is consistent

in a pure acid solution (**Fig. R 2 a-i**). Moreover, the cyclic voltammograms recorded after SEIRAS measurements at each working potential are shown in **Fig. R 3a-l**. These curves demonstrate that the Pt nanofilm electrode can endure the harsh conditions of the HER process and remains stable throughout the entire SEIRAS measurement.

Time-resolved SEIRAS spectra were also collected under potential modulation, and the generated current versus time data in the mixed solution of 0.1 M H_2SO_4 and 0.2 M K_2SO_4 at a working potential of -0.25V vs. SHE are shown in **Fig. R 4**. The charging electric quantities exceed the discharging ones, as the discharging process is affected by the hydrogen oxidation reaction (HOR) currents. Furthermore, we added time-resolved results for the IR peaks of Eigen protons to better understand the dynamic behaviors of various species at the EDL. As depicted in **Fig. R 5**, as the electrode potential shifts from PZC to a more negative potential, the IR peak of Eigen protons appears around 1500 ms and reaches its maximum at approximately 3000 ms. This process closely mirrors the dynamic contraction of the inner EDL layer, indicating a coupled relationship between the contraction of the inner EDL layer and the approach of Eigen protons to the Pt electrode, which may arrange outside the cation layer.

Supplementary Fig. S 7 - S 8 (Fig. R 1 and Fig. R 2) and **Supplementary Note 4** were added in the revised supporting information (Page 15 to 17).

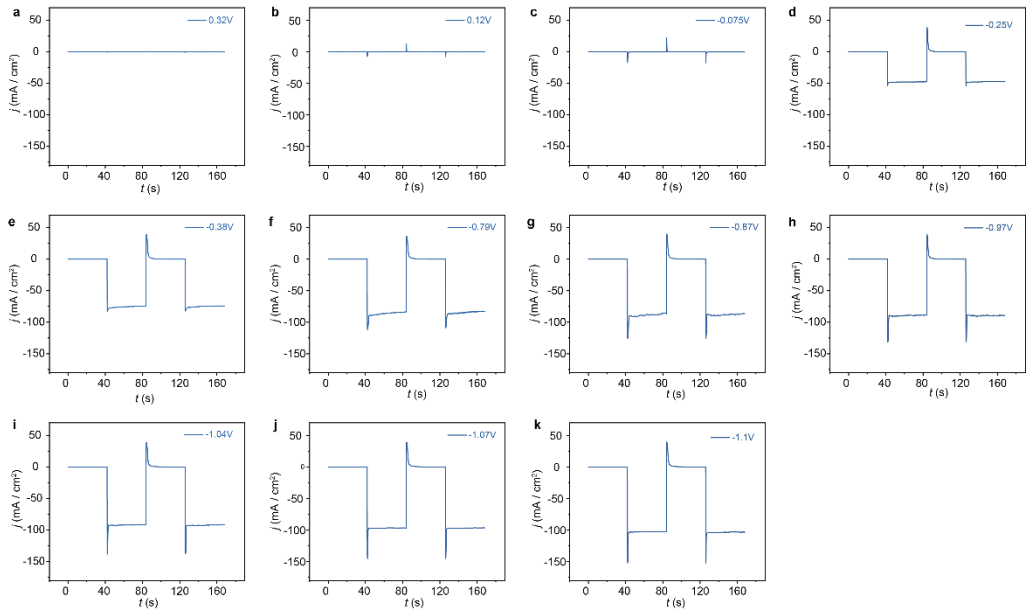


Fig. R 1. Steady-state current versus time profiles at various potentials recorded in a mixed solution of 0.1 M H_2SO_4 and 0.2 M K_2SO_4.

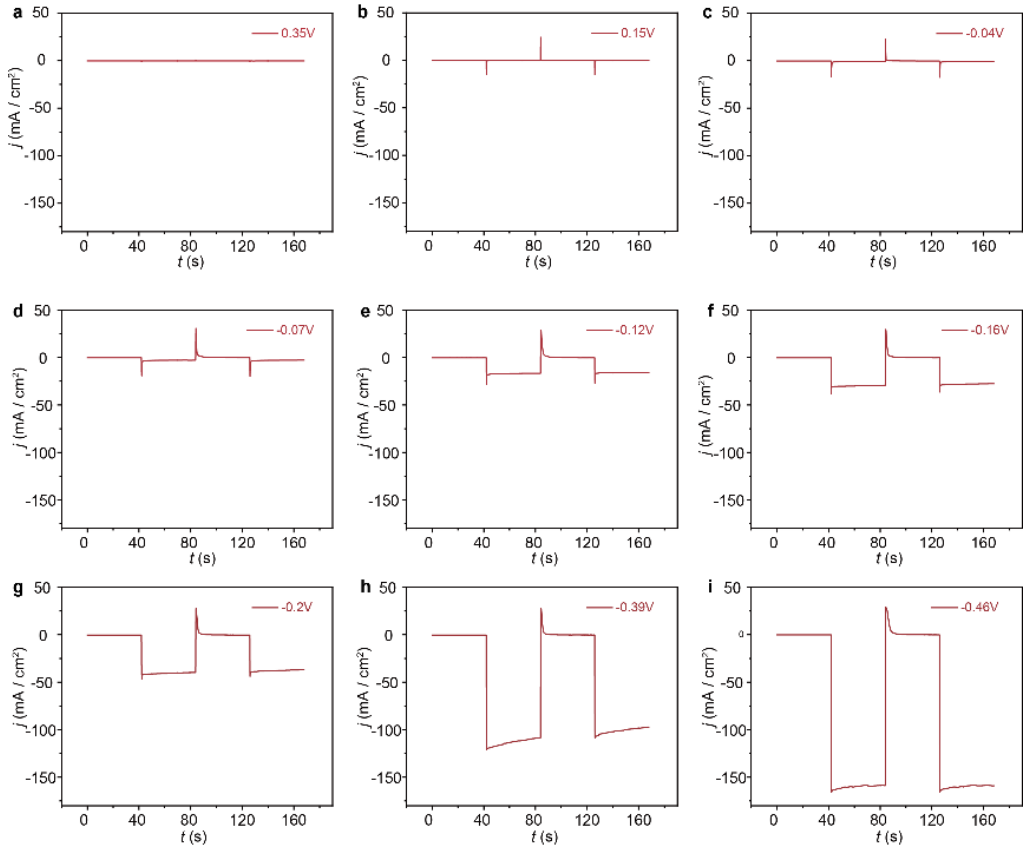


Fig. R 2. Steady-state current versus time profiles at various potentials recorded in 0.1 M H_2SO_4 solution.

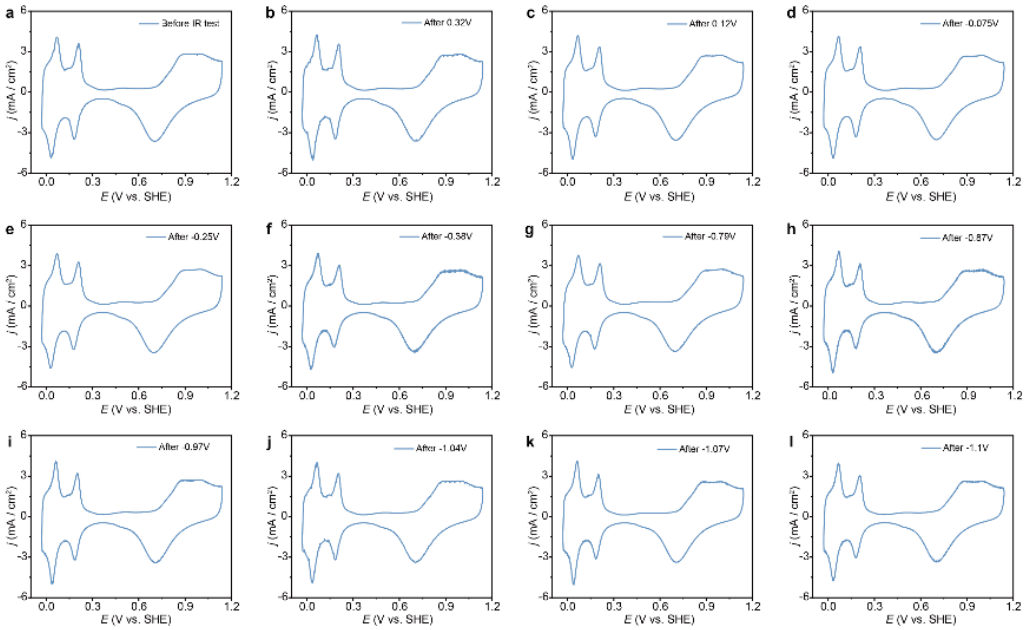


Fig. R 3. CV curves obtained after SEIRAS measurements in a mixed solution of 0.1 M H_2SO_4 and 0.2 M K_2SO_4 at various potentials.

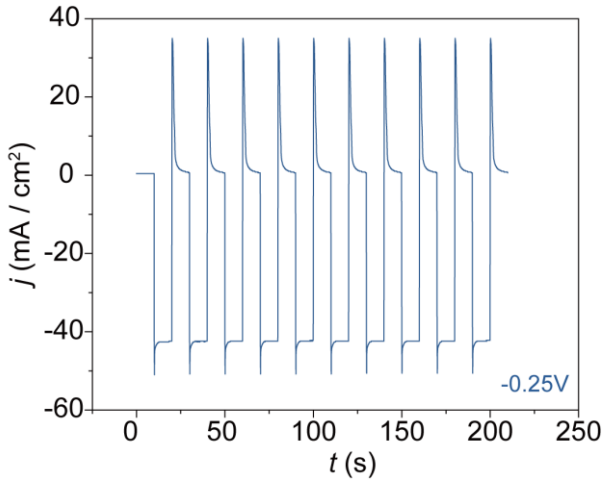


Fig. R 4. Current-time profiles recorded during time-resolved SEIRAS measurements in a mixed solution of 0.1 M H_2SO_4 and 0.2 M K_2SO_4 at a working potential of -0.25 V vs. SHE.

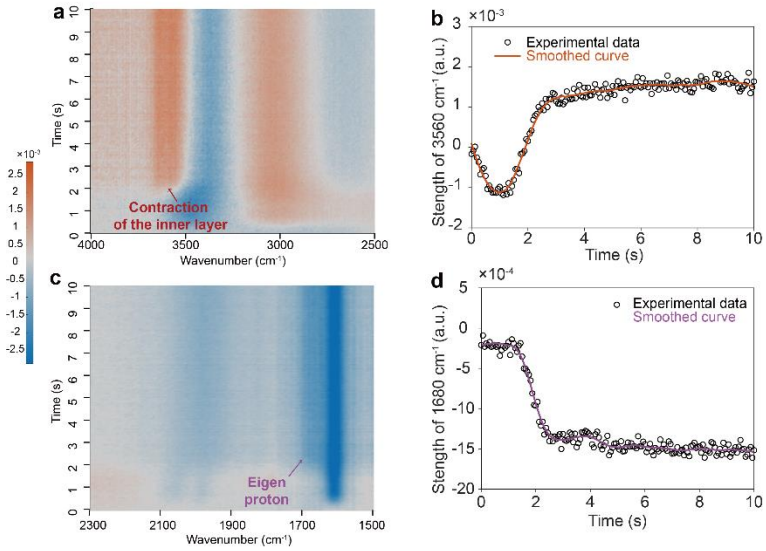


Fig. R 5. a, c, Time-resolved SEIRAS data shown across different wavenumber ranges with a time resolution of 62.5 ms. The electrode potentials are 0.37 V vs. SHE (E_R) and -1.04 V vs. SHE (E_S). **b** and **d** show the time-dependent intensity of the IR signals at 3560 cm^{-1} (**b**) and 1680 cm^{-1} (**d**), respectively.

Comment 3: The authors state, "Interestingly, the intensity of this band at 750 ms is approximately 1.5 times higher than in the steady state (>3000 ms), indicating a disordered water network in the transition state." Why is this true? More details on how this conclusion is justified would be helpful. Currently, it is stated without a detailed explanation. It is well documented that water solvated to alkali metal cations (such as sodium) exhibits an O-H vibrational frequency around 3600 cm^{-1}. Is ion-solvated water truly disordered? Furthermore, the free water mode still involves on hydrogen bonded OH molecule. The O-H vibration in "free water" is energetically uncoupled from the

H-bonded O-H group References such as Wang et al. (Nature, 2021, 600, 81-85) and Scatena et al. (Science, 2001, 292, 908-912)

Response:

We thank the reviewer for raising this important point. In principal, actually the IR feature around 3550-3650 cm^{-1} is attributed to dangling OH groups, O-H stretches not engaged in hydrogen bonding, rather than a single, well-defined water species. In steady-state IR studies, such dangling OH modes have been reported for water molecules with the hydrogen pointing toward a metal surface or located in the hydration shell of cations (e.g., Na^+)[3,6]. While frequency-based assignments, such as categorizing water into 4-HB, 2-HB, and "free" water, are conceptually useful, they can be oversimplified, as the same spectral region can arise from multiple structural configurations producing dangling OH.

In our work, transient SEIRAS measurements combined with MLMD simulations reveal that, under HER-relevant non-equilibrium conditions, rapid migration of high-concentration cations in the EDL disrupts the hydrogen-bond network. This "slicing" effect can convert some strongly or moderately H-bonded OH groups (~3400 cm^{-1}) into dangling OH groups (~3600 cm^{-1}), thereby increasing the intensity in this region during the transition state (Fig. R 6). As the EDL relaxes to steady state, cation motion slows, the hydrogen-bond network reorganizes, and the dangling OH population decreases, reducing the 3600 cm^{-1} intensity.

Thus, the observed 1.5-fold enhancement at ~750 ms reflects a transient increase in the proportion of dangling OH groups caused by dynamic cation-water interactions, rather than the emergence of a new, static water species. This multi-contributor perspective offers a more accurate interpretation of the 3550-3650 cm^{-1} region and better captures the complexity of interfacial water dynamics under reactive conditions.

In our revised manuscript, we have included the following additional discussion (Page 7 to 10) and revised **Fig 2** (Page 26 to 27) to clarify the variation in interfacial water during the process of "EDL breathing", and also added **Supplementary Fig. S 13 (Fig. R 6)** in the revised supporting information (Page 37):

"To further identify the origin of these features, we partitioned the water layer into seven distinct regions based on their proximity to the electrode surface and their association with K^+ hydration shells (Extended Data Fig 4), and extracted vibrational spectra from each region. The results show that the dominant spectral differences arise from whether water molecules reside in the inner or outer layer of the EDL. Accordingly, we separately present spectra for these regions in Fig 2c-d. The outer-layer water shows relatively weak potential dependence, with an upward peak at ~3675 cm^{-1} and a downward band near 3336 cm^{-1}. In contrast, the inner-layer water exhibits strong potential-dependent changes and clearly undergoes two-phase evolution. In the first

phase (blue curves), water molecules reorient to form more hydrogen-down configurations at the electrode surface (Fig 2e-i, Fig 2k), resulting in a downward peak around 3600 cm^{-1}, consistent with earlier observations[30]. Concurrently, the disruption of the hydrogen-bonding network leads to a decrease in tetrahedrally-coordinated (4 H-bonded) "ice-like" water[31] (Fig 2l) and an increase in less coordinated (2 H-bonded) water, contributing to the upward band at ~3000 cm^{-1} and the downward band at ~3400 cm^{-1}.

In the second phase, the interfacial structure deviates significantly from equilibrium. A distinct shift of the upward peak from 3568 cm^{-1} to 3492 cm^{-1} is observed, with intensity increasing as potential becomes more negative. This spectral evolution is attributed to the contraction of the inner layer, as captured by simulations, indicating a reduced interfacial water content (Fig 2g-j). As shown in Fig 2m, the hydration shell of K^+ remains largely unchanged during phase I but undergoes notable changes in phase II. As potential decreases, the surface coverage of K^+ increases, and its second hydration shell (~5 Å) is significantly disrupted. Simultaneously, a decrease in the first hydration shell peak suggests partial dehydration of K^+. The density distribution of K^+ and O atoms (Fig 2n) also vary depend on potentials: at moderate potentials, K^+ primarily locates 3.3 Å from the Pt electrode surface, with interfacial water distributed extensively across the EDL. As the electrode potential decreases, the radial distribution peak of K^+ shifts to 3.0 Å, while interfacial water moves farther from the electrode surface, peaking at 3.45 Å. These changes suggest a reduction in the thickness of the EDL's inner layer due to water being expelled from between the K^+ ions and the Pt surface. It is noteworthy that this interfacial cation dehydration is only partial. Driven by the strong electric field, the dehydration is anisotropic, leading to unique interfacial structures characteristic of a far-from-equilibrium state.

The dynamics of reactive EDLs were then analyzed using time-resolved SEIRAS (Fig 3, Extended Data Fig 5, Methods), which also reveal two distinct processes in the time-dependent structure evolution of EDL. When the potential is polarized from 0.37 V to -1.04 V (Fig 3a-b), the signal caused by the reorientation of water (downward signal at ~ 3600 cm^{-1}) and the disruption of H-bonding network (upward band at ~ 3000 cm^{-1}, downward signal at ~ 3450 cm^{-1}) appears rapidly before the contraction of the inner layer. Subsequently, the contraction of the inner layer occurs in a longer time scale, with the decreasing signal between 3500 cm^{-1} and 3650 cm^{-1} (upward peaks marked in orange) reaching steady state at around 2900 ms (Fig 3b). Notably, the contraction process of the inner layer of EDL with K^+ takes around thousands of milliseconds, which is longer than that of the dehydration process of hydrophobic organic cations[32]. The expansion dynamics of EDL upon potential shifts from -1.04 V to 0.37 V were also explored, exhibiting distinct features compared to the contraction process. Specifically, a downward band between 3500 cm^{-1} to 3650 cm^{-1} appears and increases rapidly within 750 ms during the expansion process (Fig 3e-f). Interestingly, the intensity of this band at 750 ms is approximately 1.5 times higher than in the steady state (> 3000 ms),

indicating a low number of hydrogen bonds in the transition state of water network. As simulations revealed (Supplementary Fig. S 13), when high-concentration cations migrate rapidly under the condition far-from equilibrium state, the movement of cations and water molecules are decoupled, cations can slice the H-bonding network and facilitate an increase in free water and exhibits the vibration feature around 3600 cm^{-1} as well. As the transient water network transits to a steady state (> 3000 ms), revealed by the decreased intensity of free water (~3600 cm^{-1}), the signal of strongly hydrogen-bonded water (~3000 cm^{-1}) appears (Fig 3e). This unique transition state of water reorganization distinguishes the expansion dynamics of EDL from the contraction process, revealing the irreversible manner for structure variation of inner layer of EDL-a phenomenon we term "EDL breathing".”

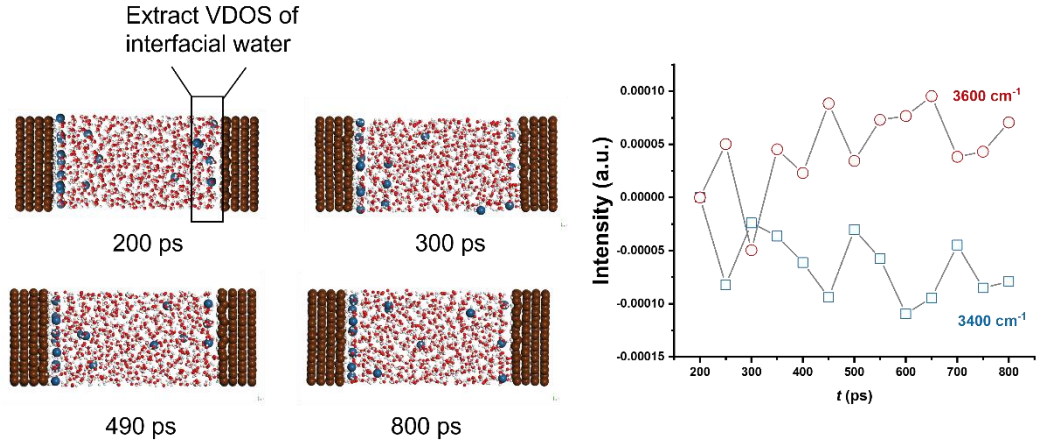


Fig. R 6 The dynamic of expansion of EDL was simulated by MLMD. The electric field was applied to drive K^+ to move from the right side to the left side. The VDOS of interfacial water on the right side was monitored, showing the intensity of vibration at 3600 cm^{-1} increase and that at 3400 cm^{-1} decrease, when K^+ migrate and slice the water network.

Comment 4: SEIRAS data collected in alkali-metal-free electrolytes down to -1.1 V, along with time-resolved measurements similar to those in Figure 2, is missing. This data is necessary to determine whether the "breathing behavior" is specific to alkali-metal-containing systems or is a general phenomenon. Additionally, it would help clarify how alkali metals influence the behavior of the interface.

Response:

We thank the referee for this valuable comment. In our original submission, time-resolved SEIRAS measurements in an alkali-metal-free electrolyte were not included. To better understand whether “EDL breathing” occurs at alkali-metal-free interfaces, we conducted new time-resolved SEIRAS experiments in 0.1 M H_2SO_4. Practical

electrode potentials were determined by precise iR correction: the measured solution resistance was 29 Ω (Gamry Interface 5000E), which, combined with the high HER current in 0.1 M H_2SO_4, results in a substantial potential drop. Consequently, the most negative practical potential achievable at the Pt nanofilm electrode was -0.46 V vs. SHE (**Table. R 1**), significantly less negative than the -1.1 V vs. SHE attainable in alkali-metal-containing systems where "EDL breathing" is observed. This limitation is inherent to the maximum output of our potentiostat (Princeton PAR-263A) and the large uncompensated resistance of the acid electrolyte.

Despite this, we performed time-resolved SEIRAS at -0.04 V and -0.20 V vs. SHE to probe interfacial water dynamics. As shown in **Fig. R 7**, the alkali-metal-free system exhibits potential-direction-dependent restructuring of the hydrogen-bond network, similar to alkali-metal-containing electrolytes near PZC. When the potential is stepped from the PZC to more negative values, protons are rapidly attracted to the Pt surface (within hundreds of milliseconds), increasing weakly hydrogen-bonded water and decreasing strongly hydrogen-bonded water. When stepped back toward the PZC, proton release into the bulk is slower, reflecting the formation of a more rigid, stable EDL at negative potentials.

Due to the experimental potential limit, we could not acquire time-resolved spectra at -1.1 V vs. SHE in the alkali-metal-free system. Within the accessible range, where "EDL breathing" does not occur, the Stark slope of Pt-H remains unchanged (**Supplementary Fig. S 19c**), indicating strong proton-water binding. This strong binding, combined with the restricted potential window, likely explains the absence of "EDL breathing" under these conditions.

Supplementary Note 10 and **Supplementary Fig. S 14 (Fig. R 7)** have been added to the revised supporting information (Page 38 to 39).

Table. R 1. The applied electrode potentials controlled by the electrochemical workstation during SEIRAS measurements in 0.1 M H_2SO_4 solution, along with the corrected electrode potentials after solution resistance compensation.

Applied electrode potential E_1 (V vs. SCE)	**Generated HER current I (mA)**	**Electrode potential after solution resistance correction E_2 (V vs. SHE)**
0.1	-0.16	0.35

-0.1	-0.2	0.15
-0.3	-0.5	-0.04
-0.35	-1.4	-0.07
-0.6	-8.1	-0.12
-0.8	-13.8	-0.16
-1	-19.2	-0.2
-2.2	-54.2	-0.39
-3	-79.3	-0.46

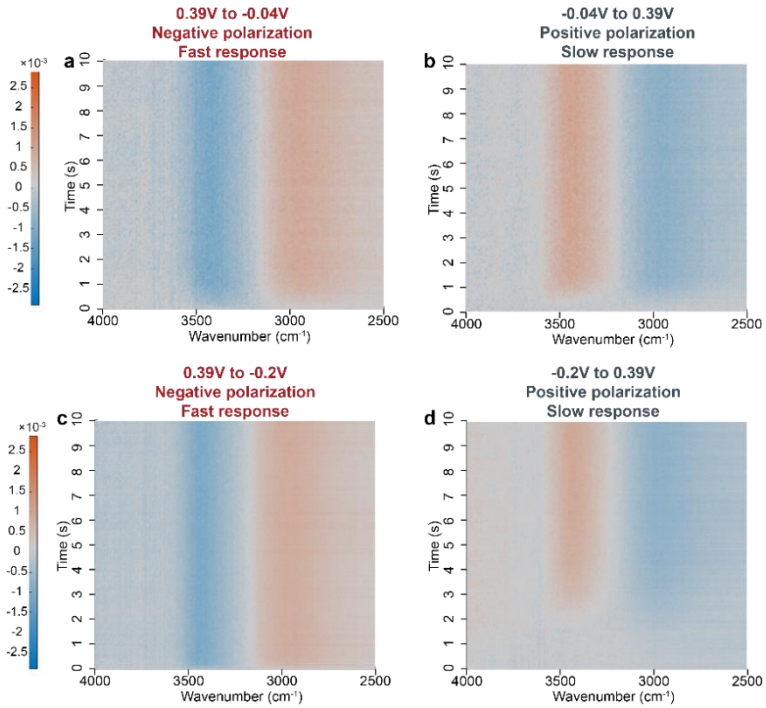


Fig. R 7. Time-resolved SEIRAS data collected in 0.1 M H_2SO_4 solution during negative polarization (**a, c**) and positive polarization (**b, d**).

Comment 5: The authors show simulated concentrations of K^+ at the outer layer and the surface in Figure 4f. What is the maximum surface coverage of cations that can be

adsorbed on the electrode under large negative bias? Does the model, which includes inner layer contraction, accurately predict these maximum coverages?

Response:

We thank the reviewer for the constructive comment. In our original submission, we did not observe the maximum coverage of K^+ because the applied electrode potentials were not negative enough to fully arrange K^+ on the Pt surface. In the revised version of manuscript, we have decreased the working potentials in SEIRAS measurements. As depicted in **Fig. R 8**, we measured the IR peaks corresponding to the first hydration shell of K^+ and the H-down water on the Pt electrode surface as the electrode potential gradually decreased. The IR signals in the 3550-3650 cm^{-1} range ceased to develop when the electrode potential reached -1.1 to -1.2 V vs. SHE for both electrolytes, confirming that K^+ had reached its maximum coverage.

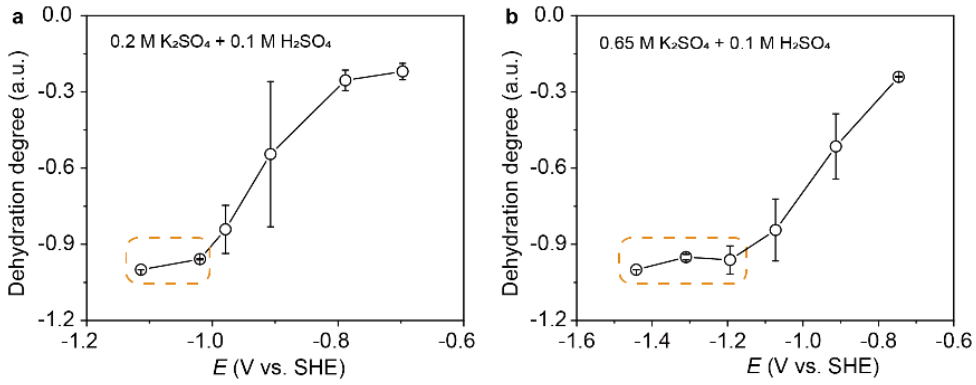


Fig. R 8. Potential-dependent intensity of IR signals in the range from 3550 to 3650 cm^{-1}, obtained from SEIRAS measurements in a mixed solution of 0.1 M H_2SO_4 and 0.2 M K_2SO_4 (a) / 0.65 M K_2SO_4 (b).

Furthermore, we employed the compressible EDL model to predict the maximum coverage of K^+. As shown in **Fig. R 9**, the concentration of K^+ no longer increases at -1.16V vs. SHE, a potential that closely matches the value deduced from the SEIRAS results. At this potential, the volume ratio of K^+ to water molecules (γ) and the thickness of the inner layer (δ) reach their limiting values, and the surface charge density as well as the interfacial electric field are at their maximum. Using the values of γ, δ, and the concentration of K^+ at -1.16V vs. SHE, we further evaluated the atomic sites occupied by K^+ as follows:

The relationship between γ and d_{K^+} is described by the following equation:

$$\gamma = \left(\frac{d_{K^+}}{d_{H_2O}}\right)^3 \quad \text{(R1)}$$

At -1.16V vs. SHE, we find γ = 1.10 and d_{H_2O} = 2.75×10^{-10} m. From this, the d_{K^+} is calculated to be 2.84×10^{-10} m.

The number of atomic sites occupied by K^+ per square centimeter on the electrode surface (N_{ads}) is calculated as:

$$N_{ads} = c_{K^+} \cdot N_A \cdot (d_{K^+} + \delta) \quad \text{(R2)}$$

Where c_{K^+} = 9.62 × 10^3 mol/m^3 and N_A is Avogadro's constant. This gives us N_{ads}=4.46 × 10^{18} sites/m^2.

To determine the K^+ coverage on the Pt electrode, we assume the Pt electrode surface to be Pt (111), which has a face-centered cubic (FCC) crystal structure. Each FCC unit cell contains four atoms, with two of them exposed on the Pt (111) surface. The edge length of the Pt (111) unit cell is denoted as a = 0.392 nm, and the unit cell has a hexagonal shape. The surface area of the unit cell A_{cell} is given by:

$$A_{cell} = \frac{\sqrt{3}}{2} a^2 \quad \text{(R3)}$$

Each unit cell exposes 2 atoms on its surface. Therefore, the surface atomic density (the number of atoms per unit area) is:

$$N_{sites} = \frac{2 \ atoms}{A_{cell}} \quad (R4)$$

Substituting a = 0.392 nm, we obtain an atomic density for Pt (111) of 1.50 × 10^{19} atoms/m^2. The number of atomic sites per square centimeter on the Pt (111) surface is approximately 1.50 × 10^{19} sites/m^2.

Based on the predictions from the compressible EDL model, the maximum K^+ coverage during EDL contraction is 29.7%, as calculated using the following equation. Interestingly, this value closely matches the maximum K^+ coverage predicted by MLMD, which is 0.23~0.24 monolayers (**Fig. R 10-Fig. R 11**).

$$\theta = \frac{N_{ads}}{N_{sites}} \quad \text{(R5)}$$

Finally, we measured Pt-D stretching frequencies as the electrode potential was decreased. As depicted in **Fig. R 9d**, at approximately -1.2 V vs. SHE, the Pt-D frequencies leveled off, indicating that the interfacial electric field no longer increased, as K^+ had reached its maximum coverage. This result aligns with the interfacial electric field predictions from the compressible EDL model (**Fig. R 9c**).

The following discussion on the maximum K^+ coverage (Page 13 to 14, Line 267 to 273) and Extended Data Fig 10 (Fig. R 9; Page 57) in our revised manuscript, with **Supplementary Fig. S 24 - Supplementary Fig. S 26** (Fig. R 10, 11 and 8) added in the revised supporting information (Page 58 to 60):

"To further verify the compressible EDL model, we extract the saturation coverage of K^+ by this continuum model (~0.29 monolayer) and MD simulations (0.23 - 0.24

monolayer), the results are consistent (Extended Data Fig 10a, Supplementary Fig. S 24-Supplementary Fig. S 25 and Table S 7). The potential to reach the saturation coverage predicted by continuum model can be further confirmed by SEIRAS measurements (Extended Data Fig 10d, Supplementary Fig. S 26).”

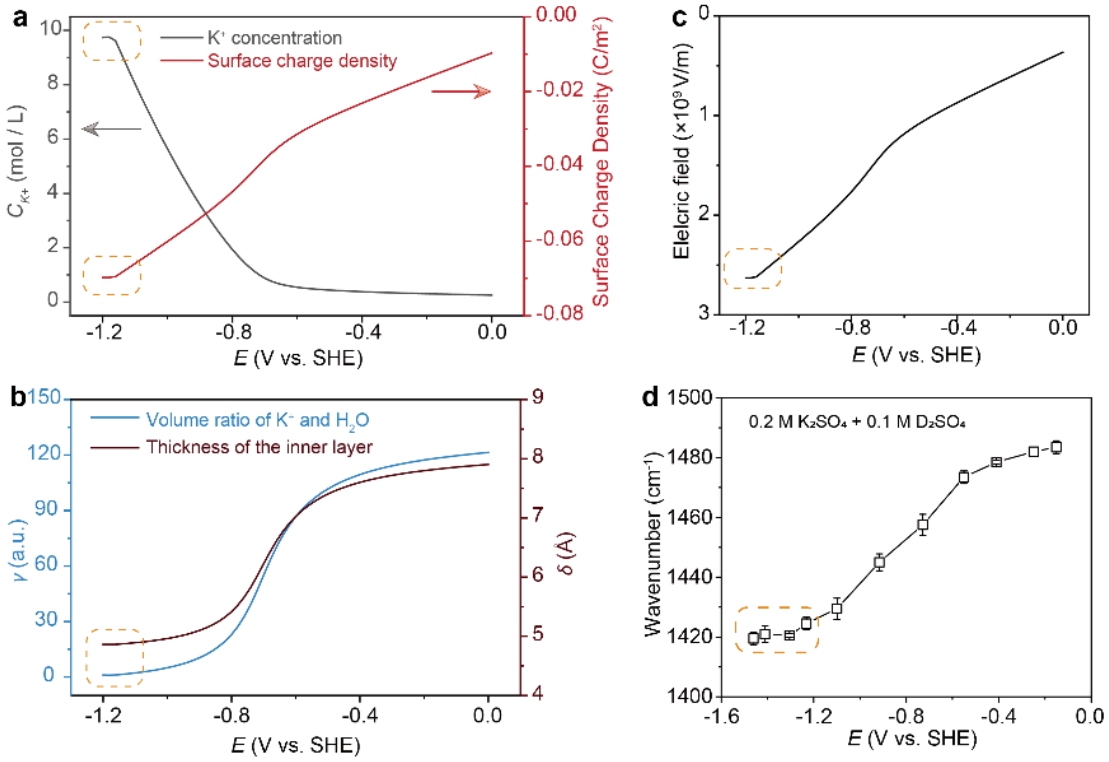


Fig. R 9. Simulated K^+ concentration and surface charge density (a) in the potential range from 0 V vs. SHE to -1.2 V vs. SHE, showing that K^+ reaches its maximum coverage on the electrode surface at -1.16 V vs. SHE. b, c, the simulated values of δ/γ (b) and the electric field intensity (c) using the compressible EDL model in the potential range from 0 V vs. SHE to -1.2 V vs. SHE. d, the measured potential-dependent Pt-D frequencies, which level off at electrode potentials below -1.2 V vs. SHE.

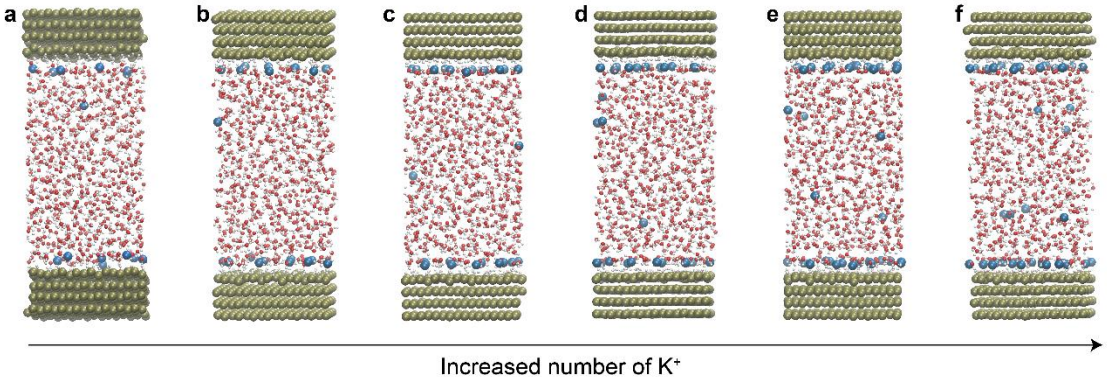


Fig. R 10. Schema of simulated MLMD models of K^+ solutions with different numbers

of K^+: a, 7 K^+; b, 10 K^+; c, 13 K^+; d, 15 K^+; e, 18 K^+; f, 21 K^+.

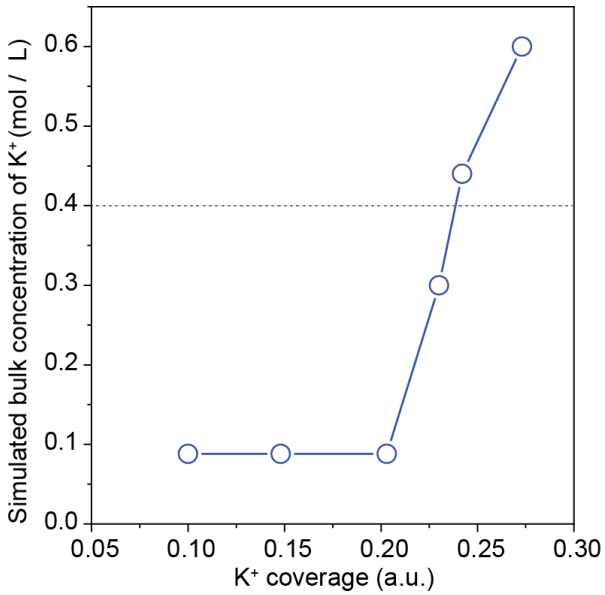


Fig. R 11. Relationship between the bulk concentration of K^+ in the simulated box and the corresponding K^+ coverage on the Pt electrode.

Comment 6: The authors observe irreversible behavior, as the water does not completely return to its original state upon reversal of the potential. Why does this irreversibility occur? Can the authors propose a hypothesis to explain this observation?

Response:

We thank the reviewer for this insightful comment. In our original manuscript, we reported that the IR signals in the 3550-3650 cm^{-1} region evolve differently during contraction and expansion of the inner layer, indicating an irreversible "EDL breathing" process. Based on our new MLMD simulations and time-resolved SEIRAS data, we can now provide a mechanistic explanation for this irreversibility.

The key lies in the fundamentally different ion-water dynamics during contraction and expansion under far-from-equilibrium conditions. In the contraction phase (potential stepped from PZC to -1.04 V), K^+ ions migrate from the diffuse layer toward the electrode. The surface ion concentration increases gradually, and the transient spectral evolution essentially follows the same sequence as the steady-state phases (phase I and phase II), involving stepwise reorientation of water molecules and progressive inner-layer compression.

In contrast, during the expansion phase (potential stepped from -1.04 V back to the PZC), the initial state is a surface saturated with K^+ at a concentration of ~8 M (**Fig. R 9a**), orders of magnitude higher than in the bulk (~0.4 M). The sudden potential

reversal causes these densely packed cations to be expelled almost instantaneously. This rapid ion release "slices" through the interfacial hydrogen-bond network, generating a transiently disordered water structure with a high proportion of dangling OH groups (~3600 cm^{-1}), shown in **Fig. R 6**. The IR intensity in the 3550-3650 cm^{-1} range thus surges to ~1.5× the steady-state value. Only after a certain relaxation period does the hydrogen-bond network reorganize and return to equilibrium.

Therefore, the observed irreversibility does not simply reflect asymmetric kinetics, but rather arises from the fundamentally different microscopic pathways: a gradual, phase-like assembly of ions during contraction versus a rapid, network-disrupting ion expulsion during expansion. This mechanistic distinction explains why the expansion phase produces a stronger transient signal and why the "EDL breathing" is inherently irreversible.

The discussion as following is added in revised manuscript (Page 9, Line 180 to 181), with **Supplementary Note 9** added in the revised supporting information (Page 35 to 36):

"Specifically, a downward band between 3500 cm^{-1} to 3650 cm^{-1} appears and increases rapidly within 750 ms during the expansion process (Fig 3e-f). Interestingly, the intensity of this band at 750 ms is approximately 1.5 times higher than in the steady state (> 3000 ms), indicating a low number of hydrogen bonds in the transition state of water network. As simulations revealed (Supplementary Fig. S 13), when high-concentration cations migrate rapidly under the condition far-from equilibrium state, the movement of cations and water molecules are decoupled, cations can slice the H-bonding network and facilitate an increase in free water and exhibits the vibration feature around 3600 cm^{-1} as well. As the transient water network transits to a steady state (> 3000 ms), revealed by the decreased intensity of free water (~3600 cm^{-1}), the signal of strongly hydrogen-bonded water (~3000 cm^{-1}) appears (Fig 3e). This unique transition state of water reorganization distinguishes the expansion dynamics of EDL from the contraction process, revealing the irreversible manner for structure variation of inner layer of EDL-a phenomenon we term "EDL breathing"."

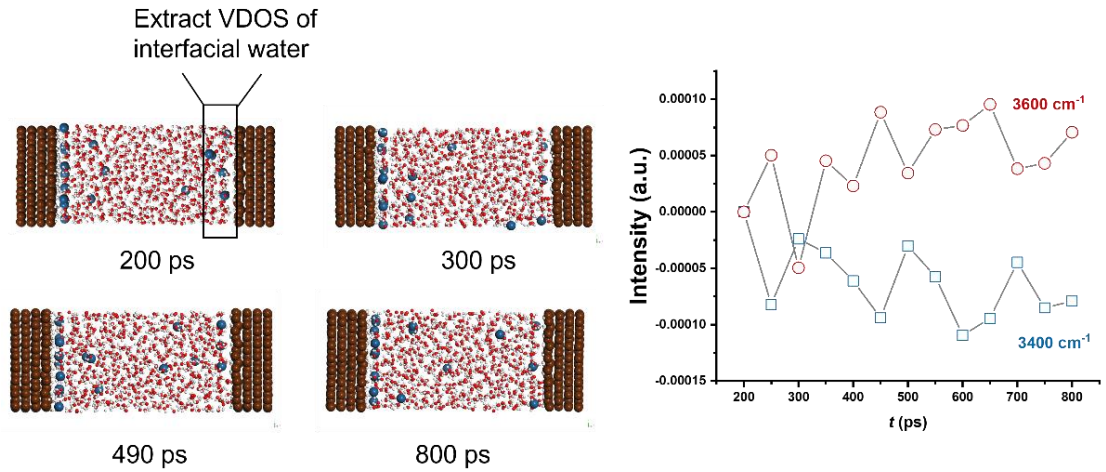


Fig. R 12 The dynamic of expansion of EDL was simulated by MLMD. The electric field was applied to drive K^+ to move from the right side to the left side. The VDOS of interfacial water on the right side was monitored, showing the intensity of vibration at 3600 cm^{-1} increase and that at 3400 cm^{-1} decrease, when K^+ migrate and slice the water network.

Comment 7: The authors discuss differences in the electric fields experienced by CO and Pt-H species on the electrode surface, yet the distance between these two molecules is not explicitly provided. Is this distance truly significant enough to account for the difference in electric field intensity? Alternatively, could the observed behavior arise from CO and Pt-H occupying distinct adsorption sites on the electrode? Furthermore, the assertion that CO coverage is only at 1% warrants clarification.

Response:

We would like to thank the reviewer for the constructive and thoughtful comments. In our original manuscript, we introduced Pt-H and CO as interfacial probes to measure the electric field intensity at different positions of the EDL. However, detailed discussions on the specific size of Pt-H and CO, the adsorption sites, and the coverage of CO were not provided. To address this, we have supplemented some SEIRAS experiments and simulations in the updated submission to thoroughly discuss above aspects. To determine the precise distances between the probes and the electrode surface, AIMD simulations were conducted for two models, with H* and CO* adsorbed on the Pt electrode surface, respectively. After the models reached equilibrium, we directly measured the distances between the Pt electrode surface and the Wannier centers of the adsorbed H and CO, which were found to be 1.27 Å and 2.27 Å, respectively. Notably, the position of Wannier center of CO between C atom and O atom is very close the plane of cations after EDL contraction that illustrated by MLMD (~3 Å, Figure 2n), indicating the adsorbed CO is very close to the position of outer layer. Consistently, as predicted by the compressible EDL model, the electric field experienced by Pt-H is

similar to that in the inner layer of the EDL, while the electric field experienced by CO is similar to that of the outer layer.

To further investigate the dynamic variations in interfacial electric field during the contraction of the inner layer at different positions of the EDL, we have introduced -SCN and $(Me)_4N^+$ as additional probes. The potential-dependent frequencies of -SCN and $(Me)_4N^+$ are shown in **Fig. R 13** and **Fig. R 14**. For -SCN, the C-N stretching frequencies decreased as the electrode potential became more negative, exhibiting a potential dependence similar to that of Pt-H and CO. Specifically, the C-N stretching frequencies displayed two distinct Stark slopes. As the electrode potential decreased from -0.08V vs. SHE to -1V vs. SHE, the Stark slope increased slightly from 9.8 $cm^{-1}V^{-1}$ to 14.5 $cm^{-1}V^{-1}$. In contrast, the C-N stretching frequencies of $(Me)_4N^+$ were independent of potential, remaining around 1481 cm^{-1} at all working potentials. As discussed in previous work, -SCN can adopt two adsorption modes: N-down and S-down[7,8]. Under our experimental conditions, the N-down and S-down adsorption modes were both observed, the frequency of which was 2069 cm^{-1} and 2116 cm^{-1}, respectively. And we use the frequency of S-down species to analyze the stark tuning rate. Combining AIMD modelling with predictions from the compressible EDL model, we found that the electric field experienced by the C-N bond of -SCN with S-down adsorption modes and $(Me)_4N^+$ corresponds to positions at 4.19 Å and 5.29 Å, respectively. As depicted in **Fig. R 14**, the distances from the probes to the Pt electrode surface follow the order: Pt-H < CO < -SCN < $(Me)_4N^+$. This trend is inversely related to the interfacial electric field intensities experienced by each probe, suggesting that the interfacial electric field strength decreases as the distance from the electrode surface increases. The variation in Stark slopes for different probes during the contraction of the inner layer is more complicated. Specifically, the enhancement amplitudes of the interfacial electric field intensities at different EDL positions follow the order: CO >> -SCN > $(Me)_4N^+$ > Pt-H. During the contraction of the inner layer, the largest increase in electric field intensity for CO located in the outer layer of the EDL can be attributed to both long-range electrostatic interactions and short-range interactions from dehydrated cations.

Table. R 2. Distances of four probes from the Pt electrode surface, computed by AIMD.

Probe	**Distance (Å)**
Pt-H	1.27
CO (adsorbed on top sites)	2.27
-SCN (S-down)	4.19

$(CH_3)_4N^+$	5.29

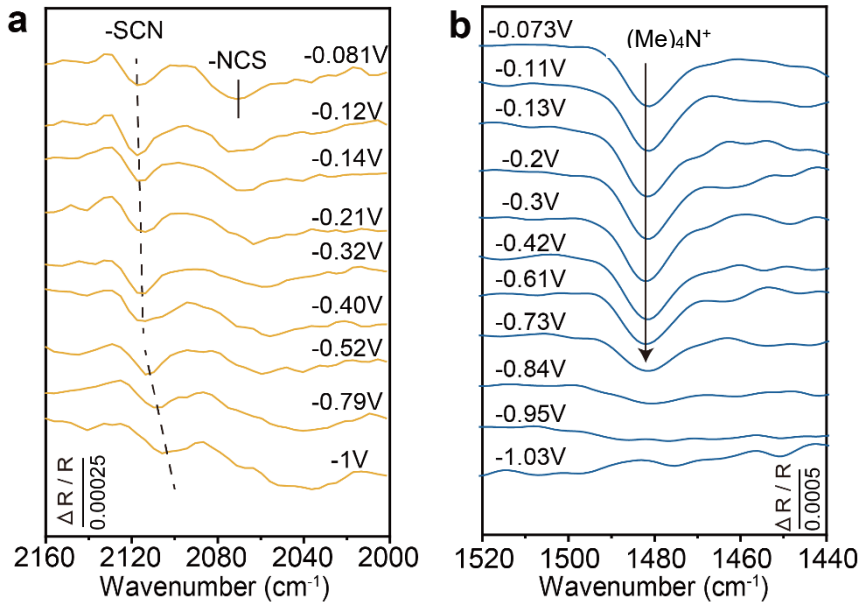


Fig. R 13. a, IR signals of -SCN and -NCS adsorbed on the Pt electrode surface, collected in a mixed solution of 0.1 M H_2SO_4 and 0.2 M K_2SO_4. b, SEIRAS results obtained in a mixed solution of 0.1 M H_2SO_4, 0.2 M K_2SO_4, and 0.05 M ammonium tetramethylsulfate. The reference potential for both measurements is 0.37 V vs. SHE.

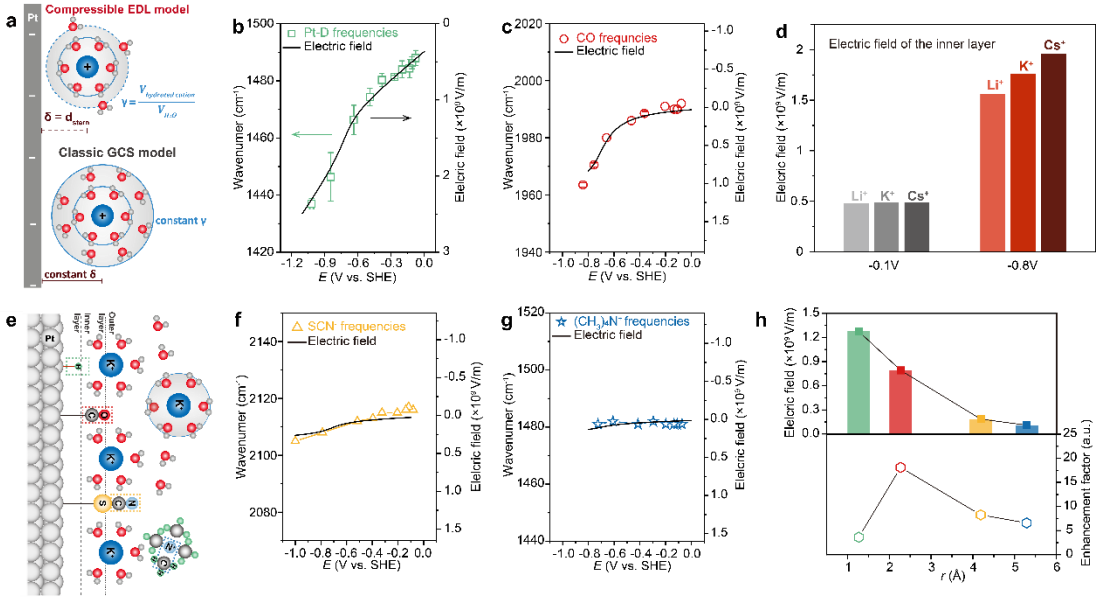


Fig. R 14. a, Comparison of measured Pt-D stretching frequencies with predicted electric field of the inner layer from the compressible EDL model. **b,** Comparison of measured CO stretching frequencies with predicted electric field of the outer layer from

the compressible EDL model. **c, d,** Comparison of measured C-N stretching frequencies of -SCN^- (**c**) and $(CH_3)_4N^+$ (**d**) with predicted electric fields at their respective positions. **e,** Schematic diagram of EDL structure with K^+ far from equilibrium, showing four probes at varying distances from the electrode. **f,** Distribution of enhanced electric field intensity and its enhancement multiple during the contraction of the inner layer across four probes at varying distances from the electrode, with potential shifts from -0.1 V vs. SHE to -0.8 V vs. SHE.

Next, we aim to determine the CO coverage by comparing the IR peak areas of the CO probe and fully adsorbed CO. The results are summarized in **Fig. R 15**, which shows that the peak areas of CO in our SEIRAS experiments and saturated CO adsorbed on Pt are 0.016 and 1.34, respectively. Based on these values, we estimate the CO coverage to be approximately 1.2%. Given that H is fully covered on the Pt electrode surface and CO coverage is nearly 1%, the most effective approach to exclude the influence of distinct adsorption sites would be to measure the potential-dependent CO stretching frequencies at various coverages. However, the IR frequency of linearly adsorbed CO is affected by coverage, as it undergoes a redshift with increasing coverage[9]. This redshift of the CO stretching frequency is attributed to the mutual effects of changes in CO binding due to coverage and dipole interactions resulting from the strong dipole-dipole coupling interaction between adsorbate molecules in the overlayer[9]. Therefore, adjusting CO coverage may not be practical in our measurement, given the additional dipole coupling effects induced by coverage changes. Therefore, in our revised manuscript, we propose an alternative method: modifying the morphology of the Pt nanofilm electrode. As shown in **Fig. R 16**, after treatment with a square wave potential shaping or re-electrodeposition, the morphology of the Pt electrode surface changes, as indicated by the comparison of CV curves. Despite these changes in morphology, the potential-dependent CO stretching frequencies during the contraction of the inner layer exhibit consistent behavior, confirming that the adsorption sites of CO do not affect the observed behavior arising from Pt-H and CO.

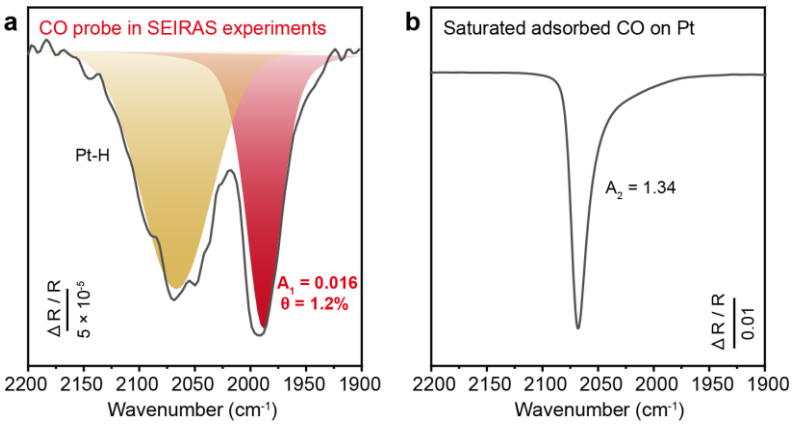


Fig. R 15. IR peak of adsorbed CO probe on Pt electrodes (**a**) and adsorbed CO with

full coverage on Pt electrode (**b**), indicating a coverage of 1.2% for CO used as probe.

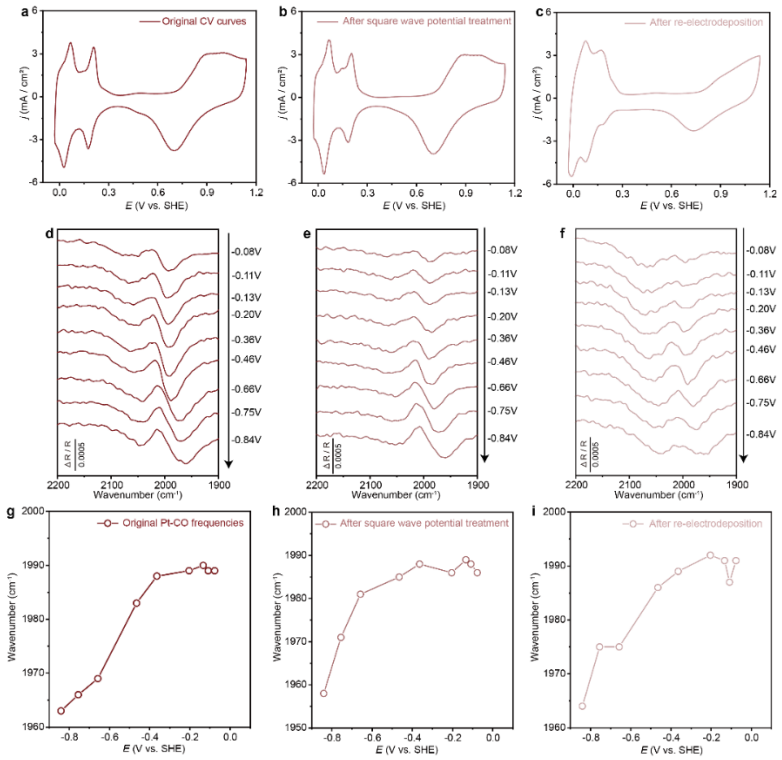


Fig. R 16. CV curves for Pt nanofilm elecreode (**a**), Pt nanofilm after square wave potential treatment (**b**) and after re-electrodeposition (**c**). IR peaks (**d-f**) and potential-dependent frequencies for CO probe (**g-i**) adsorbed on Pt electrode surfaces with different morphologies.

Revised Fig. 5 (Page 31 to Page 32) and following discussion were added in the new manuscript (Page 14 to 15, Line 286 to 302), and **Supplementary Fig. S 34** (Page 73) and **Supplementary Note 17** (Page 70 to 71) are added in the revised supporting information to discuss the data of two new probes:

"Moreover, using probes (CO, -SCN, $(CH_3)_4N^+$) with varying distances from the Pt electrode, we revealed the intensity and enhancement gradient of local electric field at different positions within the EDL across two phases (Fig 5c, e-g, Supplementary Fig. S 33, Supplementary Fig. S 34). To minimize disruption to the local water structure, CO coverage was kept below 1% (Supplementary Fig. S 35). The effect of CO adsorption configuration was excluded as well (Supplementary Fig. S 36). Potential-dependent spectra and simulations indicate that local electric field intensity inversely correlates with the distance from probe to the electrode, following the order: Pt-H > CO > -SCN > $(CH_3)_4N^+$ (Fig 5h, Table S 8). However, the enhancement factor in electric field intensity resulted from inner layer contraction is most pronounced for CO, while the other probes exhibit lower enhancement factor (Fig 5h). The reason for this phenomenon is that the CO adsorbed on the platinum surface is closest to the cation plane in the inner layer of the EDL. It is worth mentioning that Pt-H and CO serve as crucial intermediates in energy-centric reactions catalyzed at negative potentials, such

as HER and CO_2RR. The compressible EDL model provides a theoretical framework to elucidate the spatiotemporal evolution of the local electric field around key intermediates during such reactions. ”

Supplementary Fig. S 35 - Supplementary Fig. S 36 and **Supplementary Note 18** are added in the revised supporting information (Page 74 to 77) to address the effect of coverage and adsorption configuration of CO probe.

Reviewer #2:

The manuscript discusses the preparation and characterisation of platinum nanofilm electrodes for use in electrochemical measurements and surface-enhanced infrared absorption spectroscopy (SEIRAS). Using this methodology, the impact of ion interactions on the dynamics of the electric double layer during hydrogen evolution at negative potentials was studied. It particularly highlights how the presence of cations in the electrolyte influences the structure of interfacial water and the dynamics of such a structure during potential variation. The study is complemented with DFT calculations of both the double-layer structure and vibrational contributions of interfacial water and with a mean field model based on the Poisson-Boltzmann equation to explain the changes in the electric field inferred from the Stark effect on the vibrations of adsorbed hydrogens. The manuscript is well written, and the hypothesis proposed to explain the spectroscopic observations is reasonable.

Response:

We sincerely thank the reviewer for the positive feedback and valuable comments on this study.

Specific comments:

Comment 1: I have one major concern: How can the authors rule out local changes at the interphase induced by hydrogen evolution as the cause of some spectroscopic observations? I refer to bubble formation and local pH changes. Such effects should be considered with caution.

Response:

We thank the reviewer for this constructive comment. We agree with referee that local changes, such as bubble formation and pH changes due to interfacial proton consumption, may occur during our SEIRAS experiments under HER conditions. In our original submission, we did not discuss the effects of bubble formation and interfacial pH changes. In this response, we aim to address the influence of these local changes through additional experiments.

It has been proven that the departure of gas bubble is governed by the solutal Marangoni force and varies in electrolytes with different anions[10]. Specifically, in

sulfuric acid, single H_2 gas bubbles detach periodically during HER, while aperiodic detachment of small H_2 gas bubbles is observed in perchloric acid. Given the significant differences in gas bubble dynamics between sulfuric acid and perchloric acid, we repeated the SEIRAS experiments in 0.1 M $HClO_4$ solution, and a mixed solution of 0.1M $HClO_4$ and 0.4 M $NaClO_4$. The results, shown in **Fig. R 17**, indicate that the IR spectra peak characteristics remain unchanged when the anion in the electrolyte changes from SO_4^{2-} to ClO_4^-. This suggests that despite the significant differences in gas bubble dynamics between these two electrolytes, the observed phenomena in our SEIRAS measurements are not affected by the bubble formation process, indicating that bubble dynamics do not influence our measurements. To further support this argument, we repeated the SEIRAS experiments in a mixed solution of 0.1 M H_2SO_4 and 0.2 M K_2SO_4, but with altered ventilation conditions. As shown in **Fig. R 18**, the IR results remain consistent whether argon gas is bubbled into the electrolyte or not. Hence, regardless of changes in gas bubble dynamics or ventilation conditions, our SEIRAS results consistently show that bubble formation has little to no effect on the spectroscopic observations.

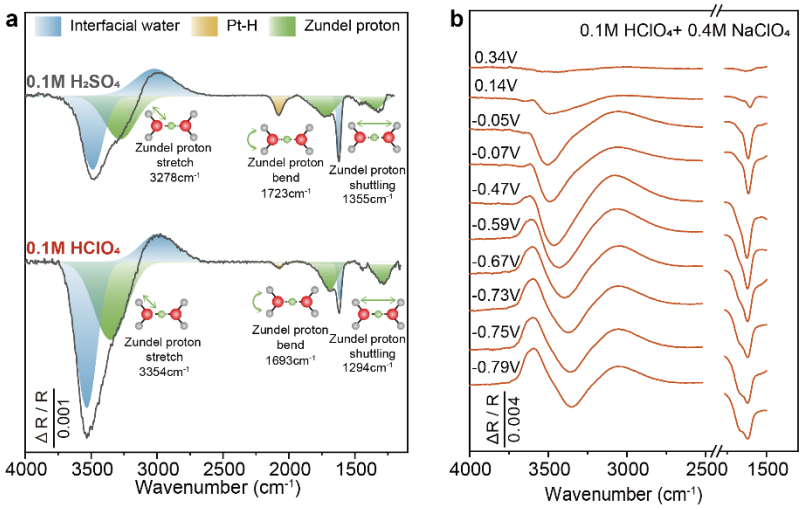


Fig. R 17. a, Infrared spectra collected in 0.1 M H_2SO_4 solution (top spectrum) and 0.1 M $HClO_4$ solution (bottom spectrum). **b,** Infrared spectra collected in a mixed solution of 0.1 M $HClO_4$ and 0.4 M $NaClO_4$, with an electrode potential of 0.39 V vs. SHE, showing that the anion has little effect on our observed phenomenon.

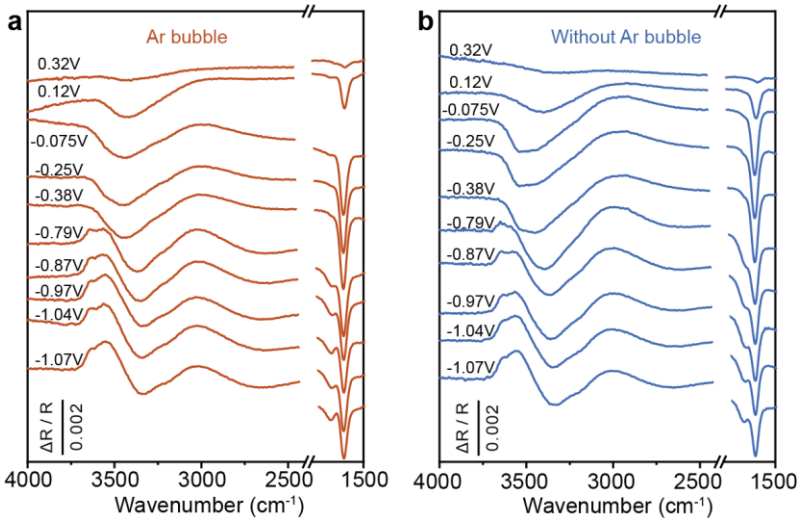


Fig. R 18. Infrared spectra collected in a mixed solution of 0.1 M H2SO4 and 0.2 M K2SO4 with Ar bubble (**a**) and without Ar bubble (**b**).

Besides, the referee raised concerns that intense HER could lead to local pH changes, potentially affecting the SEIRAS observations. In our revised version, we have addressed this concern through both theoretical and experimental analysis, demonstrating that local pH changes do not influence our findings. The key point is that interfacial charge is determined by the difference between the applied electrode potential and the electrode's point of zero charge (PZC), whereas local pH primarily influences electrochemical kinetics, rather than the interfacial electric double layer (EDL) structure. As previously reported, the PZC of Pt is pH-independent and is approximately 0.23V vs. SHE[11]. Therefore, in case of Pt electrode, while pH can affect the electrochemical reaction kinetics[12], it does not influence the EDL structure, including interfacial ion configuration and electric field distribution. In all SEIRAS measurements, our electrode potential is referenced to a saturated calomel electrode (SCE). As depicted in **Fig. R 19**, the electrode potential referenced to the saturated hydrogen electrode (SHE) remains constant provided that our applied electrode potential is fixed, regardless of pH. Therefore, in our system, the interfacial EDL structure we probed is dictated by the difference between PZC and the applied electrode potential, making it independent of pH and unaffected by local pH variations.

To support this argument, we measured potential-dependent Pt-H stretching frequencies in various electrolytes with different pH values (1.38, 7.2 and 10.91), thereby evaluating the impact of pH on the observed non-linear enhancement of the electric field during the EDL contraction process. The results, shown in **Fig. R 20**, indicate that regardless of the bulk electrolyte pH, the adsorbed H on Pt or the Pt-H stretching signal appears around RHE 0 V and becomes stable at electrode potentials below RHE 0 V (on the left side of the spectra). By converting the electrode potential from the RHE scale to the SHE scale based on the pH of each electrolyte, we can

summarize the Pt-H stretching frequencies at different electrode potentials versus SHE (on the right side of the spectra). As shown in **Fig. R 21**, despite collecting Pt-H frequencies from electrolytes with different pH values, the Stark slope of Pt-H shows the same trend observed in our working electrolyte (a mixed solution of 0.1 M H_2SO_4 and 0.2 M K_2SO_4), where it significantly increases around ~-0.6 V vs. SHE. This result demonstrates that our key spectroscopic observation, the non-linear strengthening of the interfacial electric field as the inner layer of the EDL contracts, is determined by the difference between the electrode potential and the PZC of Pt. This behavior holds true across all electrolytes, regardless of their pH. Therefore, it can be inferred that our spectroscopic observation will remain unaffected by local pH changes, as long as the applied electrode potential is kept fixed.

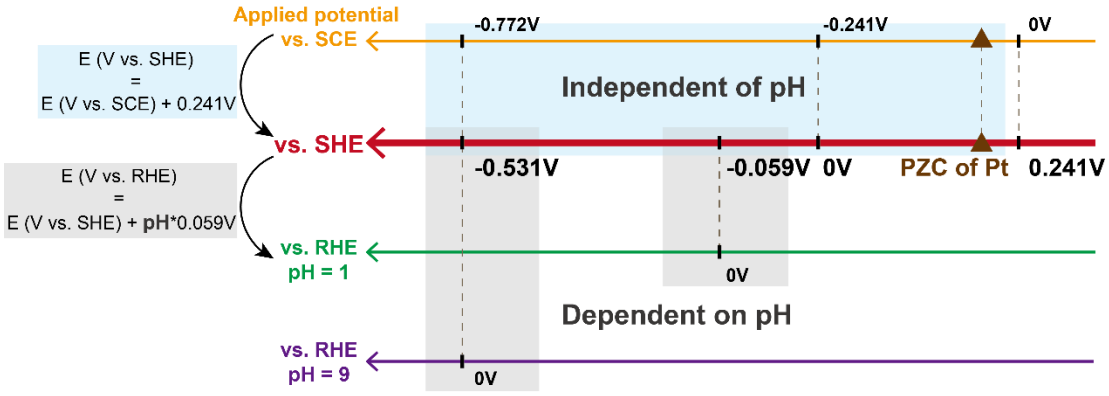


Fig. R 19. Schematic of the conversion between electrode potential and reference potential in electrolytes with different pH values.

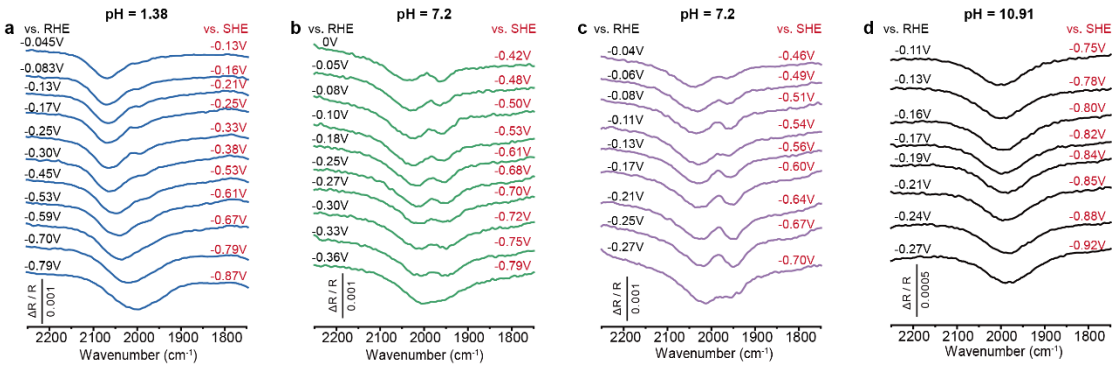


Fig. R 20. Potential-dependent IR spectra of Pt-D collected in electrolytes with pH = 1.38 (**a**), 7.2 (**b, c**), and 10.91 (**d**).

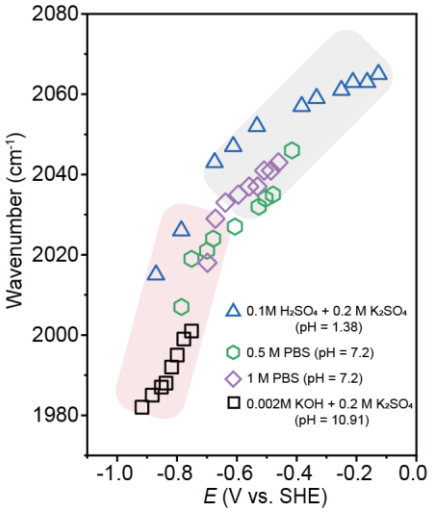


Fig. R 21. Potential-dependent Pt-D frequencies collected in various electrolytes, exhibited with reference to SHE scale.

Next, to further validate our opinion, we investigated the impact of local pH changes on spectroscopic observations during SEIRAS collection under HER conditions. We measured the CV curves of the Pt electrode in two electrolytes: 1 M phosphoric acid buffer solution (PBS) and 0.2 M K_2SO_4 solution, with the results shown in **Fig. R 22** In 1 M PBS, standard CV curves of Pt were obtained, with the hydrogen region appearing at potentials positive to apparent 0 V vs. RHE. In contrast, the CV curves for 0.2 M K_2SO_4 solution showed that the hydrogen region of Pt only appeared when the electrode potential was negative to 0 V vs. RHE, with the lower potential limit for hydrogen formation close to -0.25 V vs. RHE. This suggests that the local pH increased by more than 5 in the 0.2 M K_2SO_4 solution. Subsequently, we collected IR signals for Pt-H stretching and analyzed the potential-dependent trends of Pt-H frequencies. Consistent with the CV curves, Pt-H stretching was detected only when the electrode potential was below -0.25 V vs. RHE, confirming that the local pH in the 0.2 M K_2SO_4 solution increased during the SEIRAS measurements under HER conditions. However, the Pt-H frequencies collected in 0.2 M K_2SO_4 solution in the potential range from -0.59V vs. SHE to -1.07 V vs. SHE were in good agreement with the results obtained in other electrolytes (**Fig. R 22**), despite the significant local pH change. Therefore, both theoretical and experimental evidence demonstrate that the interfacial EDL structure and electric field primarily depend on the potential difference between the PZC of Pt electrode and the applied electrode potential, regardless of local pH.

To clarify the effect of bubble formation and local pH changes on our spectroscopic observations, we have added **Supplementary Note 13** and **Supplementary Fig. S 20 - Supplementary Fig. S 23** in the revised supporting information (Page 47 to 54), along with **Extended Data Fig 8** in the revised manuscript (Page 55).

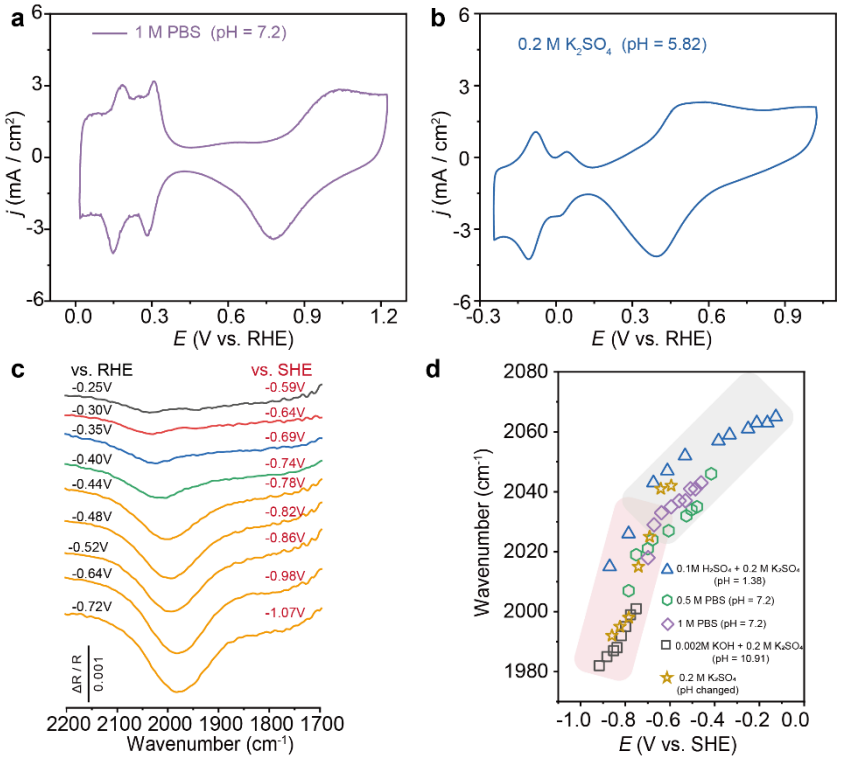


Fig. R 22. CV curves of the Pt nanofilm electrode collected in 1 M PBS solution (pH = 7.2) (**a**) and 0.2 M K_2SO_4 solution (pH = 5.82) (**b**). **c,** Potential-dependent IR spectra of Pt-D stretching obtained in 0.2 M K_2SO_4 solution (pH = 5.82). **d,** Potential-dependent Pt-D frequencies collected in various electrolytes, including 0.2 M K_2SO_4 solution (pH = 5.82), referenced to the SHE scale.

Comment 2: Other minor point are: While all potentials in the text are given with reference to the standard hydrogen electrode, the only voltammogram shown in the Supporting Information is plotted versus the calomel reference electrode. This makes it difficult to correlate the spectroscopic results with the electrochemical response of the electrode.

Response:

We would like to thank the reviewer for this thorough observation. In the revised manuscript, we have updated the reference for the cyclic voltammograms to the standard hydrogen electrode, as illustrated in **Fig. R 23** and **Supplementary Fig. S 2** in the revised supporting information.

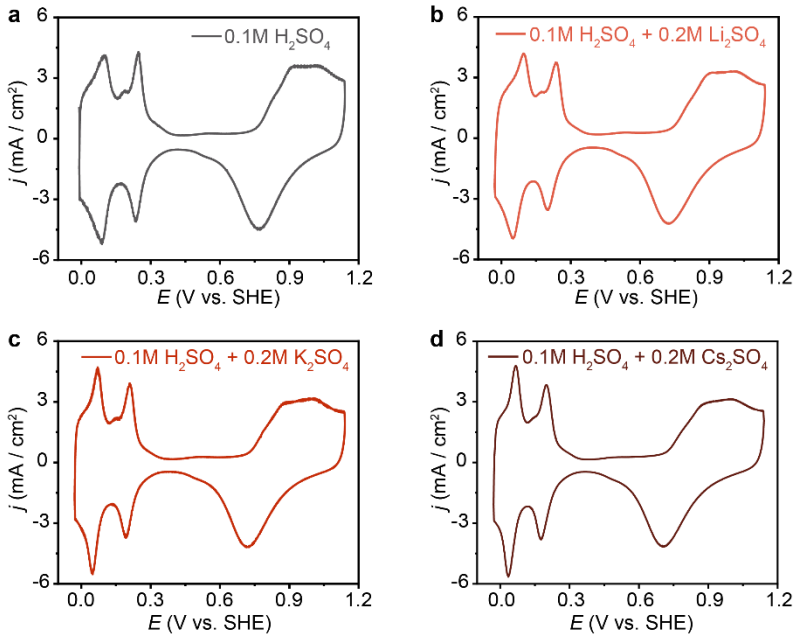


Fig. R 23. CV curves of the Pt nanofilm electrode collected in various electrolytes for SEIRAS measurements, referenced to the SHE scale.

Comment 3: While the voltammogram looks clean and compatible with a clean interphase, I am worried that some lead used in the electroplating solution might be alloyed with platinum and might affect the rate of hydrogen evolution. Have the authors checked the films for the presence of lead by XPS or related techniques?

Response:

We would like to thank the reviewer for the careful comment. In our electrodeposition method, approximately 1% wt $(CH_3COO)_2Pb$ was added to the electroplating solution to fabricate a stable Pt black nanofilm[13]. In our original submission, we did not analyze the potential amount of Pb that may have been co-deposited with Pt. To address this, we have incorporated XPS experiments in the revised manuscript to detect the presence of Pb. As shown in **Fig. R 24** and Table. R 3, we conducted two parallel XPS measurements and found that negligible Pb was detected in the Pt nanofilm formed by the square-wave electrodeposition process. Specifically, in the first test, the atomic ratio of Pt to Pb was 94.5:1, while in the second test, no Pb was detected. Based on these results, we conclude that only trace amounts of Pb are co-deposited on the Pt nanofilm, and this has no impact on the HER current. Additionally, the trace amounts of S and O detected in the XPS spectra likely originate from the residual electrolyte, 0.1 M H_2SO_4 solution, used during the modulation process with a square-wave potential.

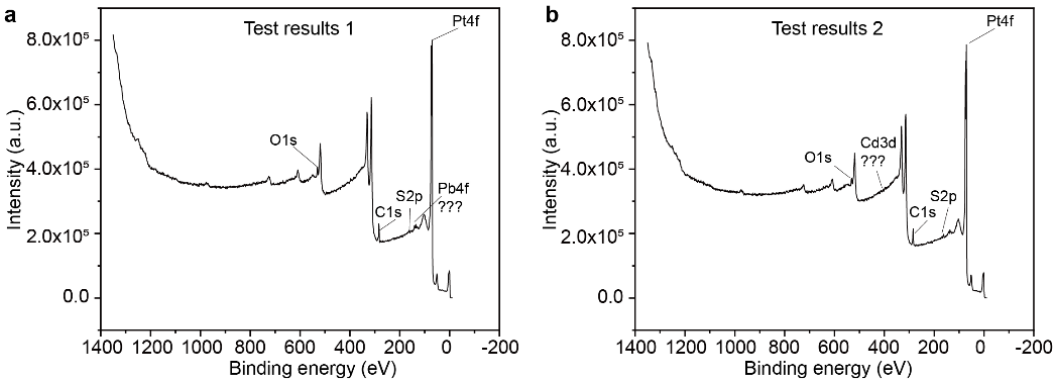


Fig. R 24. XPS results of the square-wave electrodeposited (ed) Pt black obtained in two parallel experiments.

Table. R 3. XPS data of the square-wave electrodeposited (ed) Pt black.

Testing sequence	Name	Peak position	Full width at half maximum	Peak Area	Atomic (%)
1	**Pt4f**	71.23	6.25	4284835.86	**47.25**
	C1s	283.84	3.08	195179.21	39.17
	O1s	530.33	2.00	85464.14	6.75
	S2p	162.01	3.73	62443.43	6.33
	Pb4f	136.19	3.07	89070.47	**0.50**
2	**Pt4f**	71.34	2.94	3956999.43	**47.49**
	C1s	284.23	3.09	175530.05	38.35
	O1s	531.36	3.97	80095.20	6.89
	S2p	162.34	2.04	64540.93	7.12
	Cd3d	403.95	3.28	18982.32	0.15
	Pb4f				**Not detected**

Comment 4: Finally, in Supplementary Note 7, the authors claim that both underpotential and overpotential hydrogen are visible in the spectra, while I can only see one band in the spectra. This requires clarification. Besides, the coverage of 66% that the authors mention is only valid for Pt(111), while the voltammogram shows a response corresponding to polycrystalline platinum, where coverage is close to 100%. Therefore, the reference to the value of 66% might be irrelevant in this case.

Response:

We thank the reviewer for this thoughtful comment. In **Fig. R 25a-c** and **Table. R 4**, we have shown the results of the parallel experiments conducted three times, which indicate the IR peak of Pt-H at each applied electrode potential. As the electrode potential decreases, the Pt-H peak area continuously increases and reaches its maximum at -0.17V vs. RHE, facilitating the elevated but eventually stable Pt-H coverage on the Pt electrode. In our three experiments, the Pt-H coverage at 0V vs. RHE is 68%, 60% and 72%, respectively, which averages to 66% in our original manuscript. Additionally, in 2007, Masatoshi Osawa and Keiji Kunimatsu explored hydrogen adsorption during HER using SEIRAS. Consistent with our results, they found that H adsorbed on the Pt electrode surface at top sites exhibited IR peaks at 2080-2095 cm^{-1} in sulfuric acid and perchloric acid solutions[14]. They also observed that the IR peak of Pt-H appeared at 0.1V vs. RHE and increased in intensity at more negative potentials down to -60mV (the lowest potential limited by ohmic drop). Therefore, it can be deduced that both underpotential and overpotential hydrogen exhibit the same IR frequency since both adsorb at top sites on the Pt electrode surface.

However, as the reviewer pointed out, the coverage of underpotential hydrogen to be 66% is only valid for Pt(111)[15], so our results may be a coincidence due to averaging, and the actual coverage for underpotential hydrogen on the Pt electrode surface depends on the surface morphology, which slightly varies in our three experiments.

To correct this analysis regarding underpotential hydrogen coverage on the Pt electrode surface, we removed it in the revised submission. We really appreciate the reviewer's attention to this matter, and your suggestion has helped improve the accuracy and clarity of the manuscript.

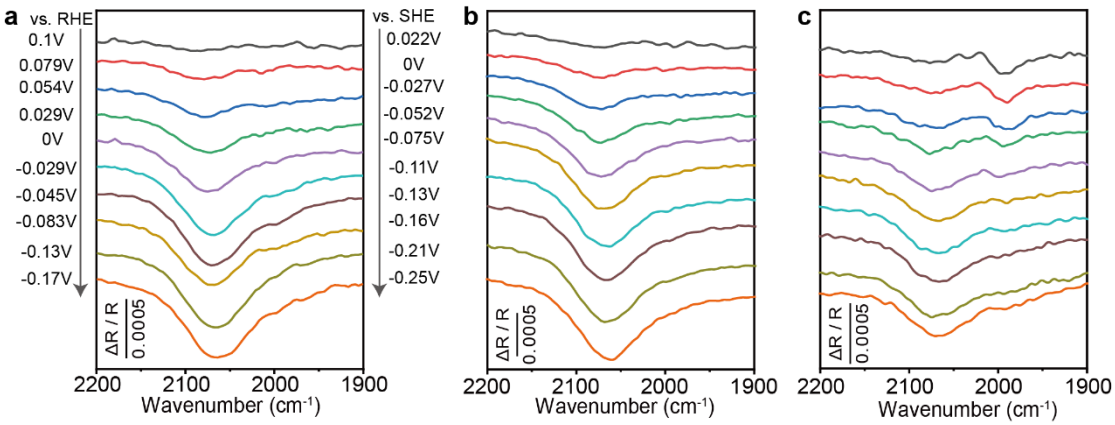


Fig. R 25. Potential-dependent IR spectra of Pt-H stretching collected three times in a mixed solution of 0.1 M H_2SO_4 and 0.2 M K_2SO_4.

Table. R 4. Collection of potential-dependent Pt-H stretching peak areas and Pt-H coverage at 0 V vs. RHE from three tests.

Electrode potential (V vs. RHE)	Electrode potential (V vs. SHE)	Normalized peak area of Pt-H in test 1	Normalized peak area of Pt-H in test 2	Normalized peak area of Pt-H in test 3	Average normalized peak area of Pt-H in three tests
0.10309	0.02209	0.07977	0.06922	0.30163	0.15021
0.07898	-0.00202	0.21449	0.17683	0.39851	0.26328
0.05413	-0.02687	0.37173	0.32716	0.57408	0.42432
0.02927	-0.05173	0.56479	0.49698	0.62598	0.56258
0.00619	**-0.07481**	**0.68154**	**0.60107**	**0.71555**	**0.66605**
-0.02864	-0.10964	0.85863	0.82706	1.03068	0.90546
-0.04549	-0.12649	0.80485	0.99061	1.02631	0.94059
-0.08342	-0.16442	0.90394	0.93846	1.09681	0.97974
-0.13093	-0.21193	1.08255	0.91566	0.94833	0.98218
-0.1696	-0.2506	1	1	1	1

Reference

1 Marcus, Y. Electrostriction in Electrolyte Solutions. *Chem. Rev.* **111**, 2761-2783 (2011).

2 Conway, B. E. Individual solvated ion properties and specificity of ion adsorption effects in processes at electrodes. *Chem. Soc. Rev.* **21**, 253-261 (1992).

3 Scatena, L. F., Brown, M. G. & Richmond, G. L. Water at hydrophobic surfaces: Weak hydrogen bonding and strong orientation effects. *Science* **292**, 908-912 (2001).

4 Davis, J., Gierszal, K., Wang, P. & Ben-Amotz, D. Water structural transformation at molecular hydrophobic interfaces. *Nature* **491**, 582-585 (2012).

5 Li, P. *et al.* Hydrogen bond network connectivity in the electric double layer dominates the kinetic pH effect in hydrogen electrocatalysis on Pt. *Nat. Catal.* **5**, 900-911 (2022).

6 Wang, Y. H. *et al.* In situ Raman spectroscopy reveals the structure and dissociation of interfacial water. *Nature* **600**, 81-85 (2021).

7 Ashley, K., Samant, M. G., Seki, H. & Philpott, M. R. Cation effects on the vibrational frequencies of adsorbed thiocyanate on platinum. *J. Electroanal. Chem.* **270**, 349-364 (1989).

8 Lu, G. *et al.* In situ FTIR spectroscopic studies of adsorption of CO, SCN^-, and poly(o-phenylenediamine) on electrodes of nanometer thin films of Pt, Pd, and Rh: Abnormal infrared effects (AIREs). *Langmuir* **16**, 778-786 (2000).

9 Olsen, C. W. & Masel, R. I. An infrared study of CO adsorption on Pt(111). *Surf. Sci.* **201**, 444-460 (1988).

10 Park, S. *et al.* Solutal Marangoni effect determines bubble dynamics during electrocatalytic hydrogen evolution. *Nat. Chem.* **15**, 1532-1540 (2023).

11 Xu, P., von Rueden, A., Schimmenti, R., Mavrikakis, M. & Suntivich, J. Optical method for quantifying the potential of zero charge at the platinum-water electrochemical interface. *Nat. Mater.* **22**, 503-510 (2023).

12 Tian, X., Zhao, P. & Sheng, W. Hydrogen Evolution and Oxidation: Mechanistic

Studies and Material Advances. *Adv. Mater.* **31** (2019).

13 Stanca, S. E. *et al.* Chemical and Electrochemical Synthesis of Platinum Black. *Sci Rep* **7**, 1074 (2017).

14 Kunimatsu, K., Senzaki, T., Samjeské, G., Tsushima, M. & Osawa, M. Hydrogen adsorption and hydrogen evolution reaction on a polycrystalline Pt electrode studied by surface-enhanced infrared absorption spectroscopy. *Electrochim. Acta* **52**, 5715-5724 (2007).

15 Markovic, N., Grgur, B. & Ross, P. Temperature-dependent hydrogen electrochemistry on platinum low-index single-crystal surfaces in acid solutions. *J. Phys. Chem. B* **101**, 5405-5413 (1997).

Referee #1:

This revision of the manuscript mostly addresses the comments and the authors give many experimental/computational data to again support their observation. There are some minor points that I would still like to point out for the authors' attention.

Comment 1:

In Figure 3, a ~800 ms temporal range is observed for Phase I-to-II transition. The authors state that this transition and related spectral data are due to inner Helmholtz plane contraction, or "breathing". With MLMD-simulated spectra, this conclusion is indeed reasonable, but in a more general physical picture, HER on Pt catalyst should mainly be a diffusion-controlled process. Thus, diffusion length can be derived from random walk process in the form of l^2~D·τ. So we can actually qualitatively evaluate the diffusion length within ~800 ms with a common D of 10-5 cm2/s, where l~28 um. This is somehow much larger than how the spatial scale of inner Helmholtz layer should be, often in Å scale. The rough estimation should remind us of considering whether EDL is actually being compressed in the inner layer or it is just reconstructuring its network. Also the contraction length is just about 2 Å from SI Fig. S 27. Though my consideration doesn't has to be completely correct, so a clarification from the authors is necessary to convince readers.

Response:

We thank the reviewer for this insightful comment. We agree that a simple diffusion-based estimate, such as $l^2 \sim D\tau$, would give a characteristic length on the micrometer scale for a time window of several hundred milliseconds. This length corresponds to the diffusion of electrolyte species involved in the surface reaction. However, the characteristic time of ~800 ms corresponding to the Phase I-to-II transition observed in Fig. 3 is not directly associated with diffusion of electrolyte species involved in the electrode reaction; instead, it shall be associated with reconstruction of the local solvation environment triggered by accumulation of spectating counterions.

After the potential step, cations first transport toward the negatively polarized Pt surface and accumulate near the interface, establishing a locally concentrated cation environment in the EDL. This initial ion-enrichment process is expected to be relatively fast. The subsequent reconstruction of the compact interfacial solvation network, involving rearrangement of interfacial water, partial dehydration of K^+, and the expulsion of water from the region between K^+ and the Pt surface, is envisioned to be slower. Because cation dehydration and water-network reorganization involve an energetic barrier, this step is not expected to follow a simple Fickian diffusion time scale.

For example, using an Eyring-type estimate, a sub-second characteristic time corresponds

to an apparent activation free energy on the order of 15 kcal mol^{-1}, which is reasonable for a barrier-limited partial desolvation/restructuring process at a highly charged interface. Therefore, the observed time constant mainly reflects the activated reorganization of the compact inner-layer solvation structure, rather than a purely diffusion-controlled HER process.

This interpretation is consistent with our MLMD simulations and compressible EDL model. As shown in Fig. 2m-o, during Phase II the K^+ hydration shell is perturbed, the K^+ density peak shifts closer to the Pt surface, and interfacial water moves away from the electrode. These changes indicate partial, anisotropic dehydration of interfacial K^+ and a reduced amount of water between the cation and the Pt surface. Thus, the "contraction" discussed in our manuscript refers to an apparent thinning/restructuring of the compact inner-layer solvation network, with an amplitude on the order of Å, rather than to a micrometer-scale diffusion within the EDL. In this picture, the transportation of ions provides the local ion enrichment, while the subsequent partial dehydration and interfacial water-network rearrangement constitute the slower, barrier-limited step.

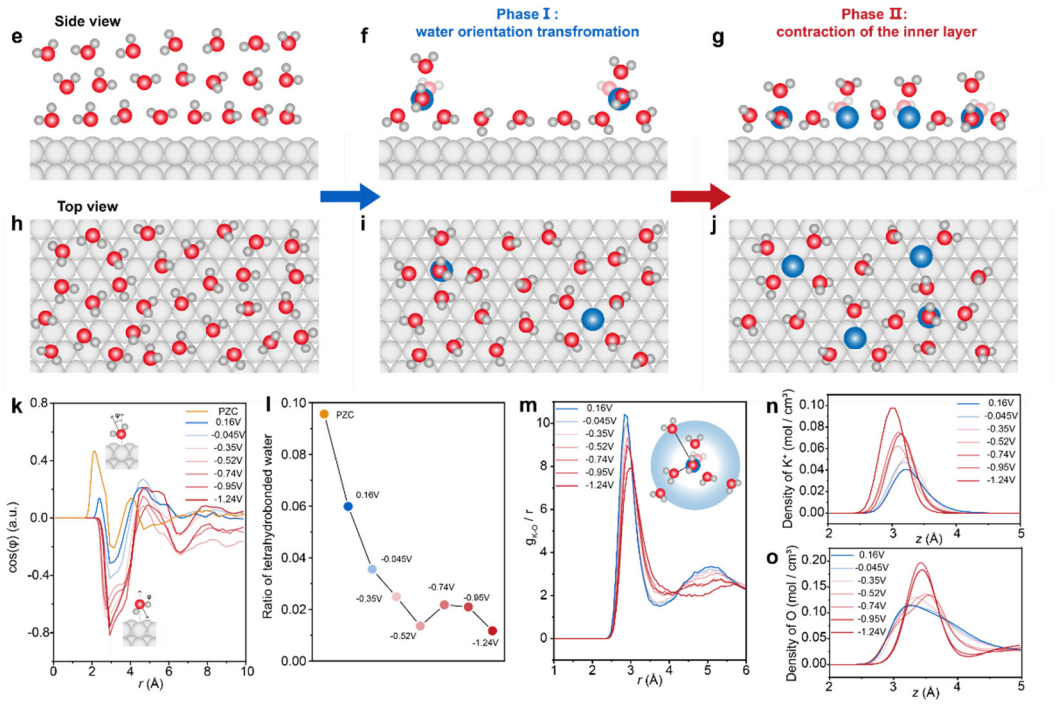


Fig. 2e-o the molecular picture of EDL contraction illustrated by MLMD.

We have added the following clarification to the revised SI as the Supplementary note 5.1: "It should be noted that the time scale of the Phase I-to-II transition should not be interpreted as a simple Fickian diffusion time corresponding to an Å-scale displacement of the IHP. Instead, after rapid ion migration/accumulation near the negatively polarized Pt surface, the observed spectral evolution mainly reflects a slower, activated reconstruction and apparent contraction

of the compact inner-layer solvation network, involving partial K^+ dehydration and rearrangement/expulsion of interfacial water. Therefore, the micrometer-scale transport length estimated from diffusion models and the Å-scale contraction length obtained from the EDL model describe different physical quantities."

Comment 2:

Other minor points are just some typos or unclear sentences in the manuscript. Line 66—an additionaly underline during sentences. "reaction conditions._Consequently, " Extended Fig 2—adding electrolyt information could be clearer for readers. SI Fig. S 4—caption and figure don't match with each other.

Response:

We thank the reviewer for pointing out these issues. We have carefully checked the manuscript and Supplementary Information and have corrected all of them accordingly.

Specifically, we have removed the extra underline/formatting mark in Line 66 around "reaction conditions. Consequently,". We have also revised the caption of Extended Data Fig. 2 by adding the electrolyte information to make the figure easier to understand. In addition, we have corrected the caption of Supplementary Fig. S4 to ensure that it accurately matches the corresponding figure.

These changes have been incorporated into the revised manuscript and Supplementary Information.

Referee #2:

The authors have convincingly addressed all of my comments. I find the paper to be robust, presenting very interesting results, and it can be published mainly in its current form. However, there is one aspect that I believe still requires clarification to enhance the manuscript's readability. This is related to the direction (positive or negative) of the vibrational bands. While the manuscript clearly states that positive bands indicate a decrease in the population of species from reference to sample potential, I feel the discussion becomes somewhat unclear at some points. For instance, the positive band at 3600 cm-1 observed during the desolvation of cations at very negative potentials should be interpreted as a signal of non-hydrogen bonded water molecules present at the reference potential, which is 0.37 V. Typically, an ice-like water structure has been reported in this potential range, and I am not aware of any previous detection of such non-bonded water around this potential. If this water signal pertain to water in the first or second solvation layer of the cation, it should be present at the reference potencial, which is slightly positive to the potential of zero charge

For instance, in page 8 we read the following paragraph: "In the second phase, the interfacial structure deviates significantly from equilibrium. A distinct shift of the upward peak from 3568 cm^{-1} to 3492 cm^{-1} is observed, with intensity increasing as potential becomes more negative. This spectral evolution is attributed to the contraction of the inner layer, as captured by simulations, indicating a reduced interfacial water content (Fig 2g-j). As shown in Fig 2m, the hydration shell of K^+ remains largely unchanged during phase I but undergoes notable changes in phase II. As potential decreases, the surface coverage of K^+ increases, and its second hydration shell (~5 Å) is significantly disrupted. Simultaneously, a decrease in the first hydration shell peak suggests partial dehydration of K^+. "As I mentioned earlier, the upward peak originates from a signal present at the reference potential. It remains unclear how the dehydration of potassium alone can account for this, given that potassium cations must be absent at the reference potential because it is above the pzc.

Appart from this clarification, the paper can be published in its present form.

Response:

We sincerely thank the reviewer for this constructive and insightful comment. We agree that the physical meaning of the positive bands in the electrochemical difference spectra should be clarified more explicitly, especially for the band in the 3600-3500 cm^{-1} region.

As correctly pointed out by the reviewer, the spectra presented in the manuscript are electrochemical difference spectra. Therefore, a positive-going band indicates that the corresponding vibrational species is less populated at the sample potential than at the reference potential. In this sense, the positive band observed in the 3600-3500 cm^{-1} region at very negative potentials indicates that such water species are present at the reference potential, 0.37 V, and

that their contribution decreases when the potential is driven into the regime where electric double-layer contraction occurs.

We appreciate the reviewer's concern that previous studies have mainly reported ice-like, strongly hydrogen-bonded interfacial water around the potential of zero charge, whereas the presence of weakly hydrogen-bonded or non-hydrogen-bonded water in this potential region has rarely been discussed. We believe this apparent discrepancy largely arises from the intrinsic limitation of potential-difference spectra. In most previous SEIRAS studies, including the seminal work by Osawa and co-workers (Ataka, et al. *J. Phys. Chem.* 100, 25, 10664-10672, 1996), the conclusion that ice-like water appears near the pzc was also derived from difference spectra. In that work, the ice-like water feature was observed at 0.5-0.8 V relative to a reference potential of 0.1 V. Therefore, those spectra demonstrate an increase in strongly hydrogen-bonded water relative to the reference state, but they do not provide a complete absolute description of all interfacial water species present at a given potential. In other words, the observation of increased ice-like water near the pzc does not exclude the coexistence of weakly hydrogen-bonded interfacial water at the same potential.

To further examine this issue, in our recent follow-up measurements we combined polarization modulation with ATR-SEIRAS, which allows the interfacial contribution to be extracted more directly by rapidly switching between p- and s-polarized light. Since the p-polarized signal contains both interfacial and bulk contributions, whereas the s-polarized signal is dominated by the bulk contribution, their difference provides an interfacial spectrum at a fixed potential without relying on potential-difference referencing. The resulting absolute interfacial spectrum, shown in **Fig. R1**, confirms that a measurable contribution from weakly hydrogen-bonded water in the 3600-3500 cm^{-1} region is still present.

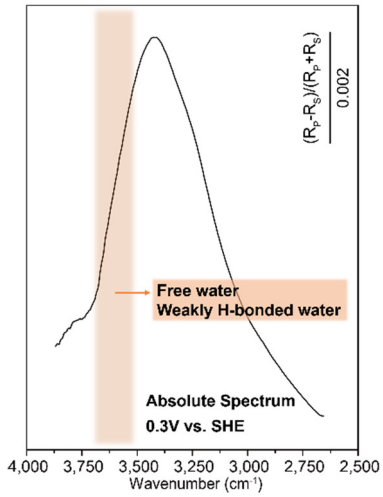


Fig. R1 polarization modulation ATR-SEIRAS to acquire water signal on Pt electrode at 0.3V vs. SHE.

We have also examined the microscopic origin of this weakly hydrogen-bonded water using

MLMD simulations at the pzc. In a simulation cell without K^+ ions, the hydrogen-bond statistics observe the presence of water molecules with a low hydrogen-bond number, for example, molecules with fewer than two hydrogen bonds **Fig. R2**. These species mainly arise from the disruption of the hydrogen-bond network by the solid-liquid interface itself. Therefore, even in the absence of specifically adsorbed or enriched cations, the interface can naturally contain a small population of weakly hydrogen-bonded water. When the inner layer of EDL contracts at very negative potentials, the number of interfacial water molecules decreases, leading to a reduction of this weakly hydrogen-bonded water signal and hence to a positive band in the difference spectrum (Fig. R2).

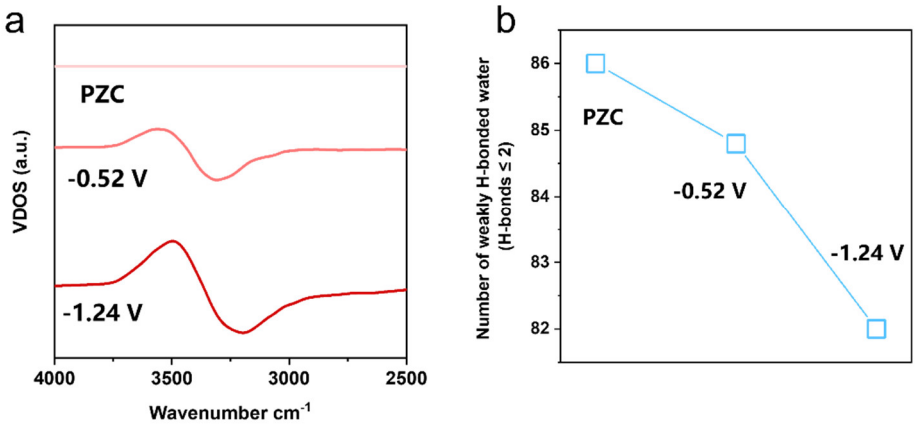


Fig. R2 (a) MLMD-simulated spectra under different potential; (b) the potential dependent trend of the content of weakly H-bonded water ($n_{H\text{-}bond} \leq 2$).

In addition, we would like to emphasize that the experimental situation at the pzc is not identical to the idealized simulation condition in which no cations are present near the interface. Experimentally, the cation concentration near the interface is not enriched at the pzc, but cations are still present at approximately bulk concentration, especially within the diffuse part of the double layer. Our CO-displacement experiments indicate that the water signal detected by PM-ATR-SEIRAS originates from a region with an effective thickness on the order of approximately 10 nm. Although only a small fraction of the water molecules within this probed region, approximately 3–5%, exhibit a pronounced potential-dependent response, the absolute spectrum at the reference potential inevitably contains contributions from water in the hydration shells of solvated K^+ ions within the probed interfacial/diffuse-layer region (~ 10 nm). Therefore, partial dehydration of K^+ at very negative potentials can also contribute to the decrease of the weakly hydrogen-bonded water signal. However, we agree with the reviewer that this contribution should not be described as if the positive band arose solely from K^+ dehydration.

Accordingly, we have added a discussion in revised SI to make the interpretation clearer. In

the revised manuscript, we explicitly state that the positive 3600-3500 cm^{-1} band reflects a decrease in weakly hydrogen-bonded interfacial water relative to the reference potential. We also clarify that this water population may originate from both intrinsically under-coordinated interfacial water and water associated with the hydration environment of K^+ within the SEIRAS probing depth. The dehydration of K^+ is therefore considered as one contribution coupled to the overall contraction and water depletion of the interfacial layer, rather than the sole origin of the positive band.

We have added Supplementary note 5.2 into revised SI: "The upward bands in the 3600-3500 cm^{-1} region correspond to water species that are more abundant at the reference potential, 0.37 V, than at the sample potential. They reflect a decrease in the population of weakly hydrogen-bonded interfacial water when the potential enters the regime of electric double-layer contraction. Although strongly hydrogen-bonded, ice-like water has commonly been reported near the pzc, this does not exclude the coexistence of a smaller population of weakly hydrogen-bonded water at the interface. Such under-coordinated water can arise from the disruption of the hydrogen-bond network by the solid-liquid interface itself, as supported by our MLMD simulations at the pzc. In addition, because the SEIRAS probing region extends into the diffuse part of the double layer, the reference spectrum may also contain contributions from water in the hydration environment of solvated K^+ ions. Therefore, the positive 3600-3500 cm^{-1} band at negative potentials is attributed to the combined decrease of under-coordinated interfacial water and hydration-shell water associated with K^+, accompanying the contraction of the inner interfacial layer and partial dehydration of K^+."